Part I

Refined Wall-Crossing

Chapter 2

Multi-Centered Black Holes and Refined Microstate Counting

As explained in the Introduction, BPS indices for Calabi-Yau threefolds can be defined in several different ways. The most physically intuitive approach uses bound states of multi-centered black holes in four-dimensional $\mathcal{N} = 2$ supergravity. This approach was developed in a series of papers by F. Denef and others [16, 57, 20], and we will follow it here to give precise definitions of BPS indices (Section 2.1) and to obtain primitive and semi-primitive wall-crossing formulas in both unrefined and refined cases (Section 2.2).

The D-brane interpretation of BPS states, and its inevitable relation to the moduli spaces of quiver representations, is still of great importance in connecting the BPS invariants of supergravity to Gromov-Witten/Donaldson-Thomas invariants and more generally to the topological invariants of Kontsevich and Soibelman [15]. It forms the basic connection between physics and mathematics. We therefore describe this interpretation, at least on a conceptual level, in Section 2.3.

We finish in Section 2.4 by exploring one of the more interesting unanswered questions about refined invariants: can they see walls in moduli spaces that are invisible to unrefined indices? We give an explicit example using internal rearrangements of multi-center black hole systems, where the naive answer is "yes," but a number of factors conspire to eliminate the presence of such walls. We conjecture that in fact the answer is always "no."

The derivation of refined wall-crossing formulas is based on our work in [1] (though it is not a far jump from the careful descriptions of wall crossing in [20]). The work on invisible

walls was done in conjunction with S. Gukov and D. Jafferis and will appear in [4].

2.1 BPS states in $\mathcal{N} = 2$ supergravity

Type II compactifications and supergravity

Generally, $\mathcal{N} = 2$ supergravity in four dimensions contains some number n_V of vector multiplets and some number n_H of (ungauged) hypermultiplets. Each vector multiplet consists of a $U(1)$ vector boson, a complex scalar, and two gauginos; while each hypermultiplet consists of two complex scalars and their spin-1/2 superpartners. Of course, $\mathcal{N} = 2$ supergravity also has a supergravity multiplet, consisting of the graviton, the gravitinos, and the graviphoton — another $U(1)$ vector boson.

Such a supergravity theory can be obtained by compactifying 10-dimensional type II string theory on a Calabi-Yau 3-fold X. The $SU(3)$ holonomy group of the Calabi-Yau ensures that exactly two supersymmetries survive the compactification. Moreover, reducing the metric, the B-field, the dilaton, and the Ramond-Ramond form fields of 10-dimensional type II supergravity via the various harmonic forms of the Calabi-Yau produces the bosonic particle content of four-dimensional supergravity. Specifically,[1] the reduction of type IIA theory results in $n_V = h^{1,1}(X)$ vector multiplets whose scalar components describe Kähler structure deformations of X; and $n_H = h^{2,1}(X) + 1$ hypermultiplets describing complex structure deformations, including the "universal hypermultiplet" that contains the 10-dimensional dilaton. In a type IIB compactification, the situation is reversed: there are $n_V = h^{2,1}(X)$ vector multiplets and $n_H = h^{1,1}(X) + 1$ hypermultiplets, again including the universal hypermultiplet that contains the dilaton.

The complex scalars of the vector multiplets and hypermultiplets are moduli of the 4-dimensional theory. Indeed, due to $\mathcal{N} = 2$ supersymmetry, the full moduli space factors exactly into vector and hyper components,

$$\mathcal{M} = \mathcal{M}_V \times \mathcal{M}_H \,, \tag{2.1.1}$$

where

$$\dim_{\mathbb{C}} \mathcal{M}_V = n_V \,, \qquad \dim_{\mathbb{C}} \mathcal{M}_H = 2n_H \,. \tag{2.1.2}$$

[1] See *e.g.* [58] and Section 9.7 of [59] for a review of type II string compactifications.

The metrics on $\mathcal{M}_V$ and $\mathcal{M}_H$ multiply the kinetic terms in the 4-dimensional Lagrangian. The hypermultiplet moduli space $\mathcal{M}_H$ is a quaternionic Kähler manifold, while the vector multiplet moduli space $\mathcal{M}_V$, which we are primarily interested in here, has special Kähler geometry [60, 61]. Thus, the geometry of $\mathcal{M}_V$ can (locally) be described using $n_V + 1$ pairs of complex special coordinates $\{X^I, F_I\}_{I=1}^{n_V+1}$, in terms of which the Kähler potential is written as

$$K = -\log i(\bar{X}^I F_I - X^I \bar{F}_I)\,. \tag{2.1.3}$$

The X^I and F_I are implicitly functions of the n_V actual complex coordinates of $\mathcal{M}_V$; locally both $\{X^I\}$ and $\{F_I\}$ form complete sets of homogeneous projective coordinates.

In a type IIB compactification, the X^I and F_I are periods of the holomorphic 3-form $\Omega \in H^{3,0}(X;\mathbb{C})$,

$$X^I = \int_{\alpha^I} \Omega\,, \qquad F_I = \int_{\beta^I} \Omega\,, \tag{2.1.4}$$

where α^I and β_I are a symplectic basis for $H_3(X;\mathbb{R})$. In a type IIA compactification, relation (2.1.4) still holds if α^I and β_I are taken to be a symplectic basis for even homology $H_{even}(X,\mathbb{R})$, and Ω is interpreted as the even form

$$\Omega = e^{-(B+iJ)} \in H^{even}(X;\mathbb{C})\,, \tag{2.1.5}$$

where B is the B-field on X and J is the Kähler class of X.

It is often useful to consider the actual metrics on $\mathcal{M}_V$ and $\mathcal{M}_H$ as "corrected" forms of much simpler metrics that are obtained in the large volume (or $\alpha' \to 0$) and weak string coupling ($g_s \to 0$) limits.[2] Because the dilaton always belongs to a hypermultiplet, only $\mathcal{M}_H$ ever receives g_s corrections (*i.e.* quantum string corrections). Similarly, because the overall volume modulus of X is a Kähler modulus, only $\mathcal{M}_V$ receives α' corrections (or worldsheet instanton corrections) in a IIA compactification, and only $\mathcal{M}_H$ receives α' corrections in a IIB compactification. Therefore, the "tree-level" geometry of $\mathcal{M}_V$ is exact in IIB string theory. Moreover, mirror symmetry relates the geometry of $\mathcal{M}_V$ in a IIA compactification on X to the geometry of $\mathcal{M}_V$ in a IIB compactification on the mirror $\tilde{X}$, and can thus be used to obtain exact metrics in type IIA as well.

[2] In fact, (2.1.5) is only true at large volume, and otherwise receives α' corrections that can be computed via mirror symmetry.

BPS states

Now consider *states* in $\mathcal{N} = 2$ supergravity. Their quantum numbers include their charges under the n_V+1 $U(1)$ vector fields (*i.e.* from the vector multiplets plus the graviphoton) and their spin. For a massive state, the spin is a half-integer describing its weight as part of a representation of the 4-dimensional massive little group $Spin(3) = SU(2)$. The electric and magnetic $U(1)$ charges can be grouped into a $2(n_V + 1)$-dimensional vector γ of integers:

$$\begin{aligned} \gamma = (p^0,\ p^A,\ q_A,\ q_0) \qquad & A = 1, ..., n_V \\ mag. \quad elec. & \\ D6\ \ D4\ \ D2\ \ D0 \quad [IIA] \quad \text{or} \quad & \text{all } D3 \quad [IIB] \\ \in H^0\ \ H^2\ \ H^4\ \ H^6(X;\mathbb{Z})\ \ [IIA] \quad \text{or} \quad & H^3(X;\mathbb{Z})\ \ [IIB] \end{aligned} \tag{2.1.6}$$

We are particularly interested in *BPS states* that preserve half of the $\mathcal{N} = 2$ supersymmetry algebra. In 4-dimensional supergravity, such states are realized as "microstates" of charged and possibly multicentered (but bound) black holes. Alternatively, in a string theory picture, these states describe D-branes wrapped on various cycles in the three-fold X and extending only along the time direction in 4-dimensional spacetime $\mathbb{R}^{3,1}$. The charges are then interpreted as D-brane charges, associated to the cycles that the D-branes wrap, as indicated in (2.1.6). By dualizing cycles to forms, the charge vector γ can also be written as a cohomology class indicated on the last line of (2.1.6). We will say more about the D-brane interpretation of BPS states in Section 2.3.

There is a natural symplectic product on charges γ in the "charge lattice" $\Gamma \simeq H^{even}(X;\mathbb{Z})$ or $H^3(X;\mathbb{Z})$, simply given by multiplying magnetic charges times electric charges:

$$\langle \gamma, \gamma' \rangle = -p^0 q'_0 - p^A q'_A + q_0 p^{0\prime} + q_A p^{A\prime} \,. \tag{2.1.7}$$

Thinking of charges γ as differential forms, this can also be written as

$$\langle \gamma, \gamma' \rangle = \int_X \gamma \wedge (\gamma')^* \,, \tag{2.1.8}$$

where the '*' is trivial in a type IIB picture, and changes the signs of 2-form and 6-form components in a IIA picture.

Attractor equations and multicentered states

The Hilbert space of BPS states, $\mathcal{H}_{BPS}$, is a piecewise-constant "function" of the vector and hypermultiplet moduli. In the particular case of vector multiplet moduli — let us denote them generically as "t" — one is free to choose any value t_∞ of moduli at spatial infinity in $\mathbb{R}^{3,1}$. Given a collection of particles (*i.e.* black holes) in $\mathbb{R}^{3,1}$, the *attractor equations* then fix the values of t everywhere else [16]. Therefore, we should write

$$\mathcal{H}_{BPS} = \mathcal{H}_{BPS}(t_\infty)\,. \tag{2.1.9}$$

The *central charge* of a state of charge γ, defined as

$$Z(\gamma;t) = e^{\frac{1}{2}K}\langle\gamma,\Omega(t)\rangle = e^{\frac{1}{2}K}\langle\gamma,(X^I(t),F_I(t))\rangle\,, \tag{2.1.10}$$

also depends on vector multiplet moduli t. (The second equality of (2.1.10) expresses Z as the product of a vector of integer charges and the vector of periods of Ω, which implicitly depend on t.) A BPS state satisfies the condition that its mass is related to the absolute value of its central charge *evaluated at moduli* t_∞,[3]

$$M = \left(m_P^{(4d)}\right)|Z(\gamma,t_\infty)| = \frac{\sqrt{\mathrm{Vol}(X)/\ell_s^6}}{g_s\ell_s}\,|Z(\gamma;t_\infty)|\,. \tag{2.1.11}$$

The phase of this central charge describes which $\mathcal{N}=1$ subalgebra of the $\mathcal{N}=2$ supersymmetry algebra the BPS state preserves. For comparison, the leading contribution (at large charge) to the entropy of a single-centered black hole of charge γ is related to its central charge when evaluated at the values of moduli $t_*(\gamma)$ *at its horizon*,

$$S \sim \pi|Z(\gamma;t_*)|^2\,. \tag{2.1.12}$$

These "attractor values" $t_*(\gamma)$ depend only on γ and not on t_∞; by the attractor equations, they minimize the central charge as a function of t.

The Hilbert space $\mathcal{H}_{BPS}$ can jump across real codimension-1 walls in $\mathcal{M}_V$, so-called walls of *marginal stability*. (It can also jump at codimension-2 loci in $\mathcal{M}_H$; this will be discussed further in Sections 2.2-2.4.) In order to understand such a transition in supergravity, one needs to consider not only single-centered black holes, but also multi-centered bound states

[3]We will henceforth set the 4-dimensional Planck mass $m_P^{(4d)} \to 1$, but remind the reader of its value in (2.1.11).

of black holes. It was shown in [16] that such stationary but non-static bound states can form from two or more black holes with mutually nonlocal charges.

To be more specific, the spherically-symmetric, static metric ansatz

$$ds^2 = -e^{2U}dt^2 + e^{-2U}d\vec{x}^2 \qquad (U = U(\vec{x})) \tag{2.1.13}$$

in $\mathbb{R}^{3,1}$ leads to attractor equations (or BPS equations) for a single-centered black hole,

$$\begin{aligned} \partial_\tau U &= -e^U|Z|\,, \\ \partial_\tau t^a &= -2\,e^U g^{a\bar{b}}\bar{\partial}_{\bar{b}}|Z|\,, \end{aligned}$$

or more compactly

$$2\,\partial_\tau \mathrm{Im}(e^{-U}e^{-i\alpha}\hat{\Omega}) = -\gamma\,. \tag{2.1.14}$$

Here, $\tau = 1/r$ is the inverse of the radial coordinate in spatial $\mathbb{R}^3$, $\alpha = \arg Z(\gamma;t)$ is the argument of the central charge, $g_{a\bar{b}} = \partial_a\bar{\partial}_{\bar{b}}K$ is the metric on $\mathcal{M}_V$, and $\hat{\Omega}(t) = e^{K/2}\Omega(t)$. In (2.1.14), one thinks of both $\hat{\Omega}$ and γ as differential forms, or, taking period integrals, as vector-valued functions. The attractor equation (2.1.14) integrates to

$$2\,\mathrm{Im}(e^{-U}e^{-i\alpha}\hat{\Omega}) = -\frac{\gamma}{r} + 2\,\mathrm{Im}(e^{-U}e^{-i\alpha}\hat{\Omega})|_{t_\infty}\,. \tag{2.1.15}$$

The resulting solution flows to a minimum of $|Z|$ as $r \to 0$.

Being slightly more careful, (2.1.15) is really only valid and describes a massive BPS black hole if $|Z(\gamma;t)|$ attains a nonzero minimum in moduli space $\mathcal{M}_V$. If $|Z|$ vanishes at a singular point in $\mathcal{M}_V$, the minimum $|Z| = 0$ can be reached at a positive radius $r = r_0$ in $\mathbb{R}^3$, and for $r < r_0$ the moduli $t(\vec{x})$ are finite constants [62, 16]. This solution is called an "empty hole." If $|Z|$ vanishes at a regular point in $\mathcal{M}_V$, the attractor equations have no solution at all.

To generalize to the multi-centered case, following [16], one replaces the metric ansatz (2.1.13) with a more general stationary metric that contains angular momentum,

$$ds^2 = -e^{2U}(dt+\omega)^2 + e^{-2U}d\vec{x}^2 \qquad (U = U(\vec{x}),\ \omega = \omega(\vec{x}))\,. \tag{2.1.16}$$

The BPS equations for a multi-centered solution with n charges γ_i at centers $\vec{x}_i$ become

$$2\,e^{-U}\mathrm{Im}(e^{-i\alpha}\Omega) = H \tag{2.1.17}$$

$$*_0\mathbf{d}\omega = \langle \mathbf{d}H, H\rangle\,, \tag{2.1.18}$$

where $\mathbf{d}$ is the exterior derivative on $\mathbb{R}^3$, $*_0$ is the Hodge dual with respect to the flat metric on $\mathbb{R}^3$, α is the argument of the *total* central charge $Z(\gamma) = Z(\gamma_1) + Z(\gamma_2) + ... + Z(\gamma_n)$, and

$$H = -\sum_{i=1}^{n} \frac{\gamma_i}{|\vec{x} - \vec{x}_i|} + 2\,\mathrm{Im}(e^{-i\alpha}\hat{\Omega})|_{t_\infty}\,. \tag{2.1.19}$$

This is not so easy to integrate directly; however, (2.1.18) implies that $\langle \Delta H, H\rangle = 0$, which does lead to integrability conditions

$$\sum_{j=1}^{n} \frac{\langle \gamma_i, \gamma_j\rangle}{|\vec{x}_i - \vec{x}_j|} = 2\,\mathrm{Im}(e^{-i\alpha} Z(\gamma_i))|_{t_\infty} \qquad \forall\, i\,. \tag{2.1.20}$$

Conditions (2.1.20) fix $n-1$ independent center-to-center radii. In particular, in the 2-centered case, the distance between black holes is completely fixed:

$$r_{12} = \frac{1}{2}\langle \gamma_1, \gamma_2\rangle \frac{|Z_1 + Z_2|}{\mathrm{Im}(Z_1 \bar{Z}_2)}\bigg|_{t_\infty}\,, \qquad Z_i \equiv Z(\gamma_i)\,. \tag{2.1.21}$$

The resulting multi-centered black holes have an intrinsic electro-magnetic angular momentum that can simply be calculated by the Poynting vector[4]; in the 2-centered case, its magnitude is just

$$J_{12} = \frac{1}{2}|\langle \gamma_1, \gamma_2\rangle| - \frac{1}{2}\,. \tag{2.1.22}$$

Note that multi-centered bound states can *only* form if charges of constituents are mutually nonlocal, *i.e.* $\langle \gamma_i, \gamma_j\rangle \neq 0$. Otherwise, the attractive force between BPS centers will completely vanish.

The supergravity picture of wall crossing, *i.e.* jumps in $\mathcal{H}_{BPS}$, involves constituents of a multi-centered bound state coming unbound, causing the state to disappear from the single-particle spectrum. From (2.1.20) or (2.1.21), it is clear that this happens when the central charges of two constituents or groups of constituents align,[5] causing a center-to-center radius to diverge. Equivalently, conservation of energy during a split of BPS states $\gamma \to \gamma_1 + \gamma_2$ requires central charges to be aligned, so that

$$\begin{aligned} &|Z(\gamma_1 + \gamma_2)| = |Z(\gamma_1) + Z(\gamma_2)| = |Z(\gamma_1)| + |Z(\gamma_2)| \\ :\qquad &M = M_1 + M_2\,. \end{aligned} \tag{2.1.23}$$

[4]Up to a quantum correction that manifests itself as the shift by $-1/2$ in (2.1.22); see [16, 57] for details.

[5]From these equations alone, it looks like anti-aligned central charges will also correspond to splits, but anti-alignment is not compatible with mass conservation.

Also observe that the alignment of central charges implies that two BPS states preserve the same $\mathcal{N} = 1$ supersymmetry subalgebra, and from basic supersymmetry considerations it is then clear that the force between them must vanish.

Indices and refinement

A useful quantity to consider in supersymmetric theories is an *index* of BPS states. In the present situation, the *second helicity supertrace*

$$\Omega(t_\infty) = -2\,\mathrm{Tr}_{\mathcal{H}_{BPS}(t_\infty)}(-1)^{2J_3}{J_3}^2 \tag{2.1.24}$$

is a good index to use. The quantum number J_3 is the half-integer $SU(2)$ spin of a given state. $\Omega(t_\infty)$ counts short BPS multiplets, and evaluates to zero on long multiplets. In particular, $\Omega(t_\infty)$ is completely invariant under a transition where short BPS multiplets combine into long multiplets and leave the BPS spectrum. Such a transition is the only type expected to occur in the moduli space $\mathcal{M}_H$ (*cf.* [21]), so the index $\Omega(t_\infty)$ is independent of hypermultiplet moduli. Of course, $\Omega(t_\infty)$ *can* jump across walls of marginal stability in $\mathcal{M}_V$ as described on page 19, where states actually disappear from the (BPS *and* non-BPS) single-particle spectrum.

One can actually do somewhat better than (2.1.24). The BPS Hilbert space is graded by charge, so one can fix a charge γ and let

$$\Omega(\gamma; t_\infty) = -2\mathrm{Tr}_{\mathcal{H}(\gamma;t_\infty)}(-1)^{2J_3}{J_3}^2\,, \tag{2.1.25}$$

where $\mathcal{H}(\gamma; t_\infty)$ is the subspace of $\mathcal{H}_{BPS}$ containing states of charge γ. Moreover, due to quantization of center-of-mass degrees of freedom (and their superpartners), all states in $\mathcal{H}_{BPS}$ have a half-hypermultiplet contribution to their spin (*cf.* [57, 11, 12, 63]). Denoting the $(2j+1)$-dimensional $SU(2)$ representation as $[j]$, this means that there is a factorization

$$\mathcal{H}_{BPS} = \left(\left[\frac{1}{2}\right] + 2[0]\right) \otimes \mathcal{H}'\,. \tag{2.1.26}$$

In terms of the reduced Hilbert space $\mathcal{H}'$, the index can be written much more simply as

$$\Omega(\gamma; t_\infty) = \mathrm{Tr}_{\mathcal{H}'(\gamma;t_\infty)}(-1)^{2J_3}\,, \tag{2.1.27}$$

where J_3 is now the spin in $\mathcal{H}'$. Note, for example, that in the reduced Hilbert space a

(half)hypermultiplet is just written as [0] and a (half) vector multiplet as $\left[\frac{1}{2}\right]$, so

$$\Omega(\text{hyper}) = 1\,, \tag{2.1.28}$$

$$\Omega(\text{vector}) = -2\,. \tag{2.1.29}$$

The indices $\Omega(\gamma; t_\infty)$ have the same continuity (and discontinuity) properties as $\Omega(t_\infty)$.

The overarching goal of Part I of this thesis is to examine the implications of *refining* this index. In other words, instead of (2.1.27), we want to take spin into account and consider

$$\Omega^{ref}(\gamma; t_\infty; y) = \mathrm{Tr}_{\mathcal{H}'(\gamma;t_\infty)}(-y)^{2J_3}\,. \tag{2.1.30}$$

The resulting refined index is a Laurent polynomial in y; it is also convenient to define its (positive integer) coefficients Ω_n as

$$\Omega^{ref}(\gamma; t_\infty; y) = \sum_{n\in\mathbb{Z}} \Omega_n(\gamma; t_\infty)\,(-y)^n\,. \tag{2.1.31}$$

Note that $\Omega^{ref}(\gamma; t_\infty; y = 1) = \Omega(\gamma; t_\infty)$. The refined index encodes much of the information present in the Hilbert space $\mathcal{H}_{BPS}$. The integers $\Omega_n(\gamma; t_\infty)$ jump across walls of marginal stability in $\mathcal{M}_V$ just as $\Omega(\gamma; t_\infty)$ does. However, they *may* also jump whenever BPS states pair up into non-BPS multiplets. We call the locations of these discontinuities "invisible walls." In the hypermultiplet moduli space they only occur at codimension-2 loci,[6] and so are not terribly offensive. Nevertheless, to be absolutely sure that the Ω_n are constant on $\mathcal{M}_H$, we should restrict ourselves to rigid Calabi-Yau manifolds (in type IIA compactifications). We investigate the possibility of encountering codimension-1 invisible walls in $\mathcal{M}_V$ in Section 2.4.

To compare to the unrefined indices (2.1.28)-(2.1.29), note that

$$\Omega^{ref}(\text{hyper}; y) = 1\,, \tag{2.1.32}$$

$$\Omega^{ref}(\text{vector}; y) = -y - y^{-1}\,. \tag{2.1.33}$$

[6]The fact that jumps in $\mathcal{M}_H$ occur at (real) codimension-2 loci rather than codimension-1 walls is related to the fact that the superpotentials in supersymmetric quantum mechanics descriptions of low-energy D-brane dynamics (*cf.* Section 2.3) are *holomorphic* functions of the hypermultiplet moduli — thus the BPS spectrum can only jump in *complex* codimension ≥ 1. Physically, these arguments also arose in the study of enhanced gauge symmetries and geometric engineering, *cf.* [21].

Topological invariants

The refined and unrefined indices of BPS states are closely related to various topological invariants of the Calabi-Yau X. Let us assume that we are in a type IIA duality frame. For a distinguished choice of t_∞ corresponding roughly to the location of the wall near large volume where $D0$ states bind to a $D6$ state, the generating function of states with $D6$-$D2$-$D0$ charges,

$$\mathcal{Z}_{D6-D2-D0}(q,Q;t_\infty) = \sum_{m\in\mathbb{Z},\,\beta\in H_2(X;\mathbb{Z})} \Omega\big(\gamma=(1,0,\beta,m);t_\infty\big)(-q)^m Q^\beta\,, \tag{2.1.34}$$

is the Donaldson-Thomas/Gopakumar-Vafa partition function for X [20]. Or, more specifically, on one side of this $D6-D0$ wall (2.1.34) is the "reduced" Donaldson-Thomas partition function $\mathcal{Z}'_{DT}$, and on the other side it is the "unreduced" Donaldson-Thomas partition function

$$\mathcal{Z}_{DT} = M(q)^{\chi(X)}\,\mathcal{Z}'_{DT}\,, \tag{2.1.35}$$

which is multiplied by an extra factor of the MacMahon function.

Similarly, the refined generating function

$$\mathcal{Z}_{D6-D2-D0}(q,Q,y;t_\infty) = \sum_{m\in\mathbb{Z},\,\beta\in H_2(X;\mathbb{Z})} \Omega^{ref}\big(\gamma=(1,0,\beta,m);t_\infty;y\big)(-q)^m Q^\beta \tag{2.1.36}$$

turns out to be equivalent to the *refined* Donaldson-Thomas partition functions defined in [23, 26] — or to Nekrasov's partition function for $\mathcal{N}=2$ gauge theory in an Omega-background [22]. We shall see an explicit example of this in Section 3.1.

In another chamber of moduli space $\mathcal{M}_V$ with strong B-field, the partition functions (2.1.34) and (2.1.36), respectively, reproduce the "noncommutative Donaldson-Thomas" invariants of Szendröi [64] and a refined version thereof.

The relation between BPS indices and (*e.g.*) topological string invariants is based on the D-brane picture of BPS states that we describe further in Section 2.3 — combined with an argument relating D-brane states with Donaldson-Thomas/Gopakumar-Vafa theory as in [20, 65]. More generally, the unrefined indices $\Omega(\gamma;t_\infty)$ in *any* chamber of $\mathcal{M}_V$ should correspond to the "classical" version of Kontsevich and Soibelman's invariants for Calabi-Yau categories [15], where t_∞ parametrizes the choice of stability condition in the category. As we explain in Chapter 4, one of our main discoveries [1] is that the refined indices

$\Omega^{ref}(\gamma; t_\infty; y)$ in turn coincide to Kontsevich and Soibelman's *motivic* Donaldson-Thomas invariants [15].

Note that all the relations we describe here are of the form $\mathcal{Z}_{BH} \sim \mathcal{Z}_{top}$, in contrast with the famed OSV conjecture $\mathcal{Z}_{BH} \sim |\mathcal{Z}_{top}|^2$ [19]. This is not inconsistent. As described in [20], the OSV relation occurs in a very special limit corresponding to highly "polar" 2-center split attractor flows which causes the BPS generating functions to factorize.

2.2 Physical wall-crossing formulas

We now proceed to take a closer look at stability conditions for BPS states, largely in a supergravity context. Following [20] (and [1]), we use physical intuition from supergravity to derive "wall-crossing formulas" that describe how refined and unrefined indices jump across walls of marginal stability in $\mathcal{M}_V$.

Stability conditions and attractor flow trees

Let us begin by considering stability of black hole states more carefully. A minimal requirement for the multi-center attractor equations (2.1.17)-(2.1.18) to have a solution is that all the radii $r_{ij} = |\vec{x}_i - \vec{x}_j|$ appearing in the integrability condition (2.1.20) are positive. Indeed, for a bound state of two black holes (or two clusters of black holes) with charges γ_1 and γ_2, positivity of the center-to-center radius (2.1.21) shows that the (potentially) stable side of a wall of marginal stability must satisfy the *Denef stability condition*

$$\boxed{\langle \gamma_1, \gamma_2 \rangle \, \mathrm{Im}\big[Z(\gamma_1, t)\overline{Z(\gamma_2, t)}\big] > 0}\,. \tag{2.2.1}$$

The codimension-1 wall of marginal stability itself is defined by the equation

$$\begin{aligned} &\arg Z(\gamma_1, t_{ms}) = \arg Z(\gamma_2, t_{ms}) \\ &\quad : \quad \mathrm{Im}\big[Z(\gamma_1, t_{ms})\overline{Z(\gamma_2, t_{ms})}\big] = 0\,. \end{aligned} \tag{2.2.2}$$

On its "unstable" side, the quantity appearing in equation (2.2.1) is negative.

While condition (2.2.1) is necessary for the formation of a stable bound state, it is not sufficient. It was conjectured in [16] (see also [66, 20]) that the multi-center attractor equations have a physically reasonable solution if and only if it is possible to draw a *split*

attractor flow tree in moduli space $\mathcal{M}_V$ starting at t_∞ and ending on "good" attractor points, *i.e.* on minima of $|Z|$ that correspond to genuine single-center black holes or empty holes. Each segment of such a tree follows a single-center attractor flow trajectory, and the flows can split at walls of marginal stability that are crossed in the stable $\rightarrow$ unstable direction. For example, single-center, two-center, and three-center flows are shown in Figure 2.1.

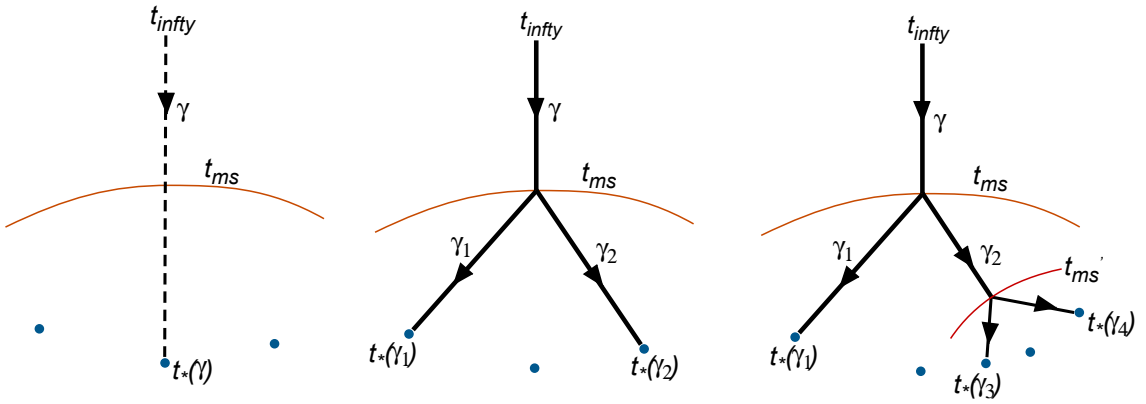

Figure 2.1: Split attractor flows in supergravity. The walls of marginal stability shown correspond to $\gamma \rightarrow \gamma_1 + \gamma + 2$ and $\gamma_2 \rightarrow \gamma_3 + \gamma_4$.

Note that flows do not *need* to split at walls of marginal stability. For example, suppose that regular positive minima (*i.e.* honest black hole solutions) exist for charges γ_1 and γ_2 on the "unstable" side of a $\gamma \rightarrow \gamma_1 + \gamma_2$ marginal stability wall, as in Figure 2.2. If a good attractor point for the total charge $\gamma = \gamma_1 + \gamma_2$ also exists on the same, unstable, side of the wall, then when t_∞ is on the stable side *both* single-center and 2-center bound states of total charge γ exist; whereas when t_∞ is on the unstable side only a single-center state of charge γ is in the spectrum. In contrast, in the case that the attractor point for $\gamma = \gamma_1 + \gamma_2$ is not a good minimum (*e.g.* if this is a regular point of moduli space with $Z(\gamma) = 0$ there), then the only possible state of total charge γ is a 2-center state that is in the spectrum on the stable side of the wall.

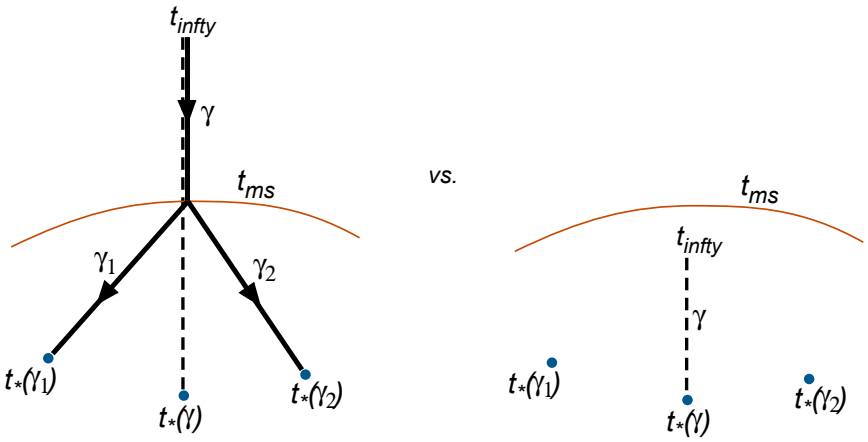

Figure 2.2: Possiblities when t_∞ is on the "stable" (LHS) and "unstable" (RHS) side of the wall.

Primitive wall crossing

We now return to the supergravity viewpoint and use physical intuition to derive *wall-crossing formulas*: formulas that describe the jumps in $\mathcal{H}_{BPS}$ and in the indices Ω and Ω^{ref} across walls of marginal stability. Many of these formulas were derived in [20]; the refined versions were also described in [67] and [1].

The simplest wall crossing scenario involves a bound state of total charge γ decomposing into two *primitive* states of charges γ_1 and γ_2 at a wall of marginal stability. Primitive means that γ_1 and γ_2 cannot be written as multiples of any smaller charge. Let the wall be at t_{ms}, and let t_+ and t_- be moduli on the stable and unstable sides of the wall, respectively. In a generic situation, $\mathcal{H}(\gamma_1)$ and $\mathcal{H}(\gamma_2)$ (and $\mathcal{H}$ for any charge that is not γ) will be continuous at t_{ms}; we may thus assume that

$$\mathcal{H}(\gamma_1; t_-) = \mathcal{H}(\gamma_1; t_+) = \mathcal{H}(\gamma_1; t_{ms})\,,$$
$$\mathcal{H}(\gamma_2; t_-) = \mathcal{H}(\gamma_2; t_+) = \mathcal{H}(\gamma_2; t_{ms})\,.$$

The separation of the bound state of charge γ into two infinitely separated black holes (or cluster of black holes) of charges γ_1 and γ_2 at t_{ms} then suggests that

$$\mathcal{H}'(\gamma; t_+) = [J_{12}] \otimes \mathcal{H}'(\gamma_1; t_{ms}) \otimes \mathcal{H}'(\gamma_2; t_{ms})\,. \tag{2.2.3}$$

This is the basis of the primitive wall-crossing formulas: the (reduced) Hilbert space on

the stable side of the wall is a product of Hilbert spaces for the components, times an electromagnetic angular momentum multiplet. Recall that the angular momentum is given by (2.1.22):

$$J_{12} = \frac{I_{12} - 1}{2}\,, \qquad I_{12} \equiv |\langle \gamma_1, \gamma_2 \rangle|\,. \tag{2.2.4}$$

Calculating the unrefined index using (2.1.27) is straightforward [20]:

$$\Omega(\gamma; t_+) = (-1)^{I_{12}-1} I_{12}\, \Omega(\gamma_1; t_{ms})\, \Omega(\gamma_2; t_{ms})\,. \tag{2.2.5}$$

Of course, there may be states of total charge γ in the BPS spectrum that do not split at the $\gamma \to \gamma_1 + \gamma_2$ wall; if so, then one should really write

$$\Delta\Omega(\gamma) \equiv \Omega(\gamma; t_+) - \Omega(\gamma; t_-) = (-1)^{I_{12}-1} I_{12}\, \Omega(\gamma_1; t_{ms})\, \Omega(\gamma_2; t_{ms})\,. \tag{2.2.6}$$

Similarly, one sees from the definition (2.1.30) that (*cf.* [67])

$$\boxed{\Delta\Omega^{ref}(\gamma; y) = [I_{12}]_{-y}\, \Omega^{ref}(\gamma_1; t_{ms}; y)\, \Omega^{ref}(\gamma_2; t_{ms}; y)}\,, \tag{2.2.7}$$

where $[I_{12}]_{-y}$ denotes the "quantum dimension"

$$[I_{12}]_{-y} = \frac{(-y)^{I_{12}} - (-y)^{I_{12}}}{(-y) - (-y)^{-1}} = (-y)^{-I_{12}+1} + (-y)^{-I_{12}+3} + ... + (-y)^{I_{12}-1}\,. \tag{2.2.8}$$

As expected, this reduces to (2.2.6) upon setting $y \to 1$.

Semi-primitive wall crossing

Now, let us view the above $\gamma \to \gamma_1 + \gamma_2$ split in reverse. As the wall of marginal stability is crossed, black holes or clusters of black holes with total charges γ_1 and γ_2 will bind to form states of total charge γ. However, the wall for $\gamma \to \gamma_1 + \gamma_2$ splits is *also* a wall for all $M\gamma_1 + N\gamma_2$ splits, with M, $N \geq 1$, and its stable and unstable sides are the same. Therefore, by the split attractor flow conjecture, bound states of any and all total charges

$$M\gamma_1 + N\gamma_2\,, \qquad M,\, N \geq 1 \tag{2.2.9}$$

should also form and be part of the BPS spectrum on the stable side of the wall. The case $M = 1$, $N \geq 1$ is called *semi-primitive* wall crossing, and can also be analyzed in the supergravity context. The general case M, $N \geq 1$ is harder to consider in supergravity, and

is most easily handled via the general Kontsevich-Soibelman wall-crossing formula that is described in Chapter 4.

During the semi-primitive splits $\gamma \to \gamma_1 + N\gamma_2$, the decomposition of the Hilbert spaces can be written as [20]

$$\bigoplus_{N=0}^{\infty} \mathcal{H}'(\gamma_1 + N\gamma_2; t_+)\, x^N = \mathcal{H}'(\gamma_1; t_{ms}) \otimes \bigotimes_{k=0}^{\infty} \mathcal{F}\left(x^k \left[J_{\gamma_1, k\gamma_2}\right] \otimes \mathcal{H}'(k\gamma_2; t_{ms})\right). \tag{2.2.10}$$

On the LHS, we have grouped all the Hilbert spaces $\mathcal{H}'(\gamma_1 + N\gamma_2; t_+)$ into a generating function. On the RHS, we consider all possible ways to bind arbitrary numbers of bound clusters of total charges γ_2, $2\gamma_2$, etc. to a γ_1 center at marginal stability (see the schematic in Figure 2.3). For each k, what is essentially a free gas of particles with charges $k\gamma_2$ are bound; $\mathcal{F}(\cdots)$ is a Fock space that describes the Hilbert space of this gas, taking into account the angular momentum contribution

$$J_{\gamma_1, k\gamma_2} = \frac{k\, I_{12} - 1}{2}, \qquad I_{12} = |\langle \gamma_1, \gamma_2 \rangle|, \tag{2.2.11}$$

and keeping track of total charge by weighing each particle with a variable x^k.

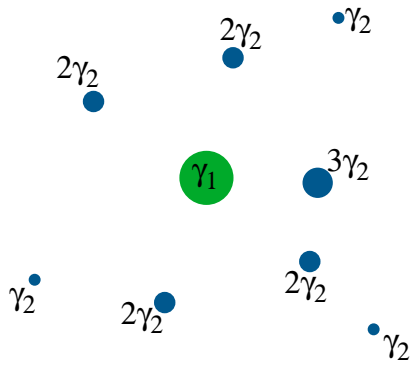

Figure 2.3: A "gas" of black holes with charges $k\gamma_2$ binding to a γ_1 center in physical space.

The resulting wall-crossing formula for unrefined indices is [20]

$$\Omega(\gamma_1; t_{ms}) + \sum_{N=1}^{\infty} \Omega(\gamma_1 + N\gamma_2; t_+)\, x^N = \Omega(\gamma_1; t_{ms}) \prod_{k=1}^{\infty} \left(1 - (-1)^{kI_{12}} x^k\right)^{kI_{12}\Omega(k\gamma_2; t_{ms})}. \tag{2.2.12}$$

The product on the RHS corresponds directly to the free gasses of particles mentioned above; the particles can be bosonic or fermionic, according to the sign of the exponent

$\Omega(k\gamma_2;t_{ms})$. In the refined case, the formula reads [1]

$$\Omega^{ref}(\gamma_1;y)+\sum_{N=1}^{\infty}\Omega^{ref}(\gamma_1+N\gamma_2;t_+;y)\,x^N \\ =\Omega^{ref}(\gamma_1;y)\prod_{k=1}^{\infty}\prod_{j=1}^{kI_{12}}\prod_{n\in\mathbb{Z}}\left(1+(-1)^n(-y)^{2j-kI_{12}-1+n}x^k\right)^{(-1)^n\Omega_n(k\gamma_2)}, \quad (2.2.13)$$

where the unambiguous moduli t_{ms} of $\Omega^{ref}(\gamma_1;t_{ms};y)$ and $\Omega^{ref}(k\gamma_2;t_{ms};y)$ have been suppressed. In the refined formula, the spin content has simply been distributed over the factors on the RHS.

Similarly to the unrefined case, formulas (2.2.12) and (2.2.13) are strictly only valid when $\mathcal{H}'(\gamma_1+N\gamma_2;t_-)$ is trivial for all $N\geq 1$ on the unstable side of the wall. If states with total charge $\gamma_1+N\gamma_2$ already exist on the unstable side of the wall, they will also bind gasses of $k\gamma_2$ particles. Then, for example, the unrefined formula reads

$$\Omega(\gamma_1)+\sum_{N=1}^{\infty}\Omega(\gamma_1+N\gamma_2;t_+)\,x^N \\ =\left[\Omega(\gamma_1)+\sum_{N=1}^{\infty}\Omega(\gamma_1+N\gamma_2;t_-)\,x^N\right]\times\prod_{k=1}^{\infty}\left(1-(-1)^{kI_{12}}x^k\right)^{kI_{12}\Omega(k\gamma_2)}, \quad (2.2.14)$$

and the refined formula generalized in an analogous fashion.

Derivation

For completeness, we finish this section by providing a derivation of the slightly non-trivial formula (2.2.13) (from which (2.2.12) also follows by setting $y\to 1$). The derivation utilizes standard techniques from statistical mechanics. It is easy to see that tracing over the LHS of (2.2.10) with weight $(-y)^{2J_3}$ gives

$$\Omega^{ref}(\gamma_1;y)+\sum_{N=1}^{\infty}\Omega^{ref}(\gamma_1+N\gamma_2;t_+;y)\,x^N\,, \quad (2.2.15)$$

and tracing over the RHS gives

$$\Omega^{ref}(\gamma_1;y)\prod_{k=1}^{\infty}\mathrm{Tr}_{\mathcal{F}^{(k)}}(-y)^{2J_3^{(k)}}x^{k\mathcal{N}}\,, \quad (2.2.16)$$

where each operator $J_3^{(k)}$ measures spin in the Fock space $\mathcal{F}^{(k)}\equiv\mathcal{F}\left(x^k[J_{\gamma_1,k\gamma_2}]\otimes\mathcal{H}'(k\gamma_2)\right)$ and $\mathcal{N}$ is the excitation number in this Fock space. We introduce quantum numbers $n_j=$

$-\frac{kI_{12}-1}{2}, ..., \frac{kI_{12}-1}{2}$ and $n \in \mathbb{Z}$, respectively, to keep track of the electromagnetic angular momentum and the internal spin of a state in the Hilbert space $[J_{\gamma_1,k\gamma_2}] \otimes \mathcal{H}'(k\gamma_2)$. For fixed n_j and n, the degeneracy of such a state is $\Omega_n(k\gamma_2)$, so we can introduce a third quantum number $m = 1, ..., \Omega_n(k\gamma_2)$ to keep track of this. The total spin is $J_3^{(k)}(n_j, n, m) = n_j + \frac{n}{2}$. Note that states with odd n are bosonic and states with even n are fermionic [20]. States in the *Fock* space $\mathcal{F}^{(k)}$ are described by entire sets of occupation numbers $\{d_{n_j,n,m}\}$, where $d_{n_j,n,m} \in \{0, 1\}$ if the state is fermionic and $d_{n_j,n,m} \in \{0, 1, ..., \infty\}$ if the state is bosonic. Thus, we have

$$\begin{aligned}
\mathrm{Tr}_{\mathcal{F}^{(k)}}(-y)^{2J_3^{(k)}} x^{k\mathcal{N}} &= \sum_{\text{sets}\,\{d_{n_j,n,m}\}} (-y)^{\sum_{n_j,n,m} d_{n_j,n,m}(2n_j+n)} x^{k\sum_{n_j,n,m} d_{n_j,n,m}} \\
&= \prod_{n_j,n,m} \sum_{d_{n_j,n,m}} (-y)^{d_{n_j,n,m}(2n_j+n)} x^{kd} \\
&= \Bigg(\prod_{n_j,n\,\text{even},m} \sum_{d=0}^{1} (-y)^{d(2n_j+n)} x^{kd} \Bigg) \times \Bigg(\prod_{n_j,n\,\text{odd},m} \sum_{d=0}^{\infty} (-y)^{d(2n_j+n)} x^{kd} \Bigg) \\
&= \Bigg(\prod_{n_j,n\,\text{even},m} \left(1 + (-y)^{2n_j+n} x^k\right) \Bigg) \times \Bigg(\prod_{n_j,n\,\text{odd},m} \left(1 - (-y)^{2n_j+n} x^k\right)^{-1} \Bigg) \\
&= \prod_{n_j,n,m} \left(1 + (-1)^n (-y)^{2n_j+n} x^k\right)^{(-1)^n} \\
&= \prod_{n_j,n} \left(1 + (-1)^n (-y)^{2n_j+n} x^k\right)^{(-1)^n \Omega_n(k\gamma_2)} \\
&= \prod_{j=1}^{kI_{12}} \prod_{n\in\mathbb{Z}} \left(1 + (-1)^n (-y)^{2j-kI_{12}-1+n} x^k\right)^{(-1)^n \Omega_n(k\gamma_2)} .
\end{aligned}$$

In the last step, we replaced n_j with the integral summation variable $j = 1 + \frac{kI_{12}-1}{2} + n_j$ to obtain the final answer.

2.3 BPS states of D-branes

The Hilbert space $\mathcal{H}'_{BPS}$ also has a description in terms of D-brane states, which is perhaps more common in the literature, and more intuitive in a string theory picture. Moreover, this description connects the supergravity picture that we have used heretofore with topological string invariants, melting crystals (Chapter 3), and the Kontsevich-Soibelman wall-crossing formulas (Chapter 4).

Roughly speaking, $\mathcal{H}'_{BPS}(\gamma)$ can be obtained in string theory compactified on a Calabi-Yau threefold X the following way. As explained in Section 2.1, charges $\gamma \in \Gamma$ can be naturally interpreted as charges of D-branes that wrap cycles of X and fill only the time direction of $\mathbb{R}^{3,1}$. In the case of type IIA theory, these are even-dimensional (holomorphic) cycles, while in type IIB theory they are odd dimensional (special Lagrangian) cycles. Fixing γ, one constructs the classical moduli space $\mathcal{M}(\gamma)$ of D-branes with this charge γ. $\mathcal{M}(\gamma)$ describes (*e.g.*) deformations of the D-branes and Wilson loop degrees of freedom on the branes. The quantum Hilbert space $\mathcal{H}'_{BPS}(\gamma)$, then, is just generated by the cohomology $H^*(\mathcal{M}(\gamma))$ as long as this cohomology makes sense[7] (*cf.* [21]). In particular, the unrefined index is an Euler characteristic and the refined index is a Poincaré polynomial:

$$\Omega(\gamma) = \chi(\mathcal{M}(\gamma))\,, \tag{2.3.1}$$

$$\Omega^{ref}(\gamma) = (-y)^{-\frac{\dim(\mathcal{M})}{2}} \text{Poincaré}(\mathcal{M}(\gamma); -y)\,. \tag{2.3.2}$$

Note that $\mathcal{M}(\gamma)$ is always Kähler, so $H^*(\mathcal{M}(\gamma))$ is organized into representations of an $SU(2)$ Lefschetz action. These coincide with the $SU(2)$ spin representations of states in $\mathbb{R}^{3,1}$, so that cohomological degree becomes identified with spin (see, for example, [57, 20, 65]). The middle cohomology (spin zero) actually corresponds to fermionic states in $\mathbb{R}^{3,1}$ once center-of-mass degrees of freedom are included; then $H^{\dim(\mathcal{M})/2+2n}(\mathcal{M})$, $n \in \mathbb{Z}$, is fermionic and $H^{\dim(\mathcal{M})/2+2n+1}(\mathcal{M})$ is bosonic. Of course, $\mathcal{M}(\gamma)$ and all related quantities depend on vector multiplet moduli, because these affect the *stability* condition for BPS branes.

We proceed to discuss some aspects of the D-brane $\leftrightarrow$ supergravity correspondence, including the inevitable realization of D-brane moduli spaces by quiver representations. We maintain the discussion at a conceptual level; for precise details we refer the reader to the references cited herein.

Quiver representations

The moduli space $\mathcal{M}(\gamma)$ of D-branes can often be described as a moduli space of quiver representations. Let us take a moment to explain what this means mathematically (see *e.g.*

[7] Generically, $\mathcal{M}(\gamma)$ is highly singular and $H^*\mathcal{M}(\gamma)$ is *not* well-defined. This is where motivic invariants become important, as described in Chapter 4. This "subtlety" is irrelevant for the present discussion, however.

[68] for a more thorough description).

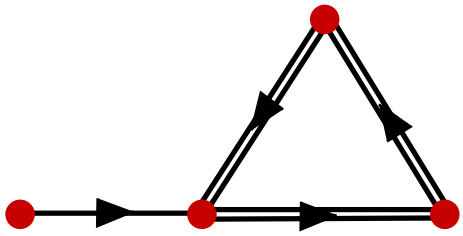

Figure 2.4: An example of a quiver with four nodes.

A quiver, as in Figure 2.4, is a collection of nodes labelled by $i \in I$ with a collection $\mathcal{A}$ of arrows connecting them. A *representation* of the quiver — or more precisely a representation of the path algebra generated by the arrows — is a collection of complex vector spaces $\{V_i\}_{i\in I}$ and a collection of homomorphisms from V_i to V_j for each arrow going from node i to node j. A quiver with closed loops can also have a superpotential W, which is a polynomial in the noncommutative arrow variables $a \in \mathcal{A}$. A representation must then obey the condition that the homomorphism corresponding to $\partial_a W$ vanishes for any $a \in \mathcal{A}$; in other words, it is a representation of the quotient of the path algebra $\mathcal{A}/dW$. There are fairly obvious notions of subrepresentations and isomorphism of representations for quivers. The latter is generated by a collection of automorphisms $g_i \in GL(V_i)$, one for each node V_i.

There is also a notion of stability for quivers called *θ-stability* [69]. For a given representation V of a quiver, let $\mathbf{n} = (n_i)_{i\in I}$ be its dimension vector, such that $n_i = \dim V_i$. Let $\boldsymbol{\theta} = (\theta_i)_{i\in I}$ be a collection of real numbers. Then a representation is θ-stable if every nontrivial proper subrepresentation $\tilde{V}$ with dimension vector $\tilde{\mathbf{n}}$ satisfies

$$\boldsymbol{\theta} \cdot \tilde{\mathbf{n}} < \boldsymbol{\theta} \cdot \mathbf{n}\,. \tag{2.3.3}$$

For a given choice of $\boldsymbol{\theta}$, we let $\mathcal{M}_s(\mathbf{n};\boldsymbol{\theta})$ be the moduli space of stable representations with dimension vector $\mathbf{n}$, modulo isomorphism — *i.e.* a quotient of all possible representations by the isomorphism group $\prod_i GL(V_i)$.

Quivers, D-branes, and supergravity

The relation between quivers, D-branes, and BPS states in supergravity is nicely described by Denef in [57]. The transition between a D-brane description and a supergravity

description is a smooth one, induced by varying the string coupling g_s. At large $g_s|\gamma|$, a BPS state of charge γ is best described as a backreacting, multi-center, solitonic black hole in supergravity, whereas at small $g_s|\gamma|$ this state is best described as a bound state of D-branes living at a *single* point in $\mathbb{R}^3$. There is no contradiction between the multi-center supergravity state and the single-center D-brane bound state: the 4-dimensional Planck length

$$\ell_P^{(4)} = \frac{\ell_s g_s}{\sqrt{\mathrm{Vol}(X)/\ell_s^6}}\,, \tag{2.3.4}$$

which sets the separation between black hole centers, becomes smaller than the string length at small g_s, so that the centers effectively fuse together.

The resulting single-center collection of bound D-branes is held together by open strings stretched between the branes. Suppose that each distinct D-brane (say D_i) supports a rank-n_i vector bundle. The low-energy dynamics of this collection can be described in nice cases by a (0+1)-dimensional supersymmetric $\prod_i U(n_i)$ gauge theory (reduced to the common noncompact worldvolume of the branes), whose matrix-valued fields describe the open string excitations between pairs of branes. The classical moduli space of this gauge theory, $\mathcal{M}_{QM}$, is equivalent to the classical moduli space of the D-branes. $\mathcal{M}_{QM}$ is obtained by solving the F-term equations $dW = 0$ as well as one D-term equation for every distinct D-brane involved in the bound state. Each D-term equation depends on a FI parameter θ_i, and the values of these parameters are a reflection in the gauge theory of the stability condition in supergravity.

It was shown by [69] that the moduli space of such a supersymmetric gauge theory is equivalent (for generic choices of $\boldsymbol{\theta}$) to the moduli space of θ-stable quiver representations with $\boldsymbol{\theta}$ set equal to the FI parameters. The relevant quiver is simply constructed by associating a node i to every $U(n_i)$ gauge field, and arrows from node i to node j to every bifundamental field representing string states from brane D_i to brane D_j. The net number of arrows between i and j is the same as the intersection number between the corresponding D-brane charges, $\langle\gamma_i, \gamma_j\rangle$.[8] The superpotential for the quiver is the same as the superpotential in the gauge theory. One then looks for θ-stable representations of the quiver with

[8]It is easy to see that this should be the case in a IIB compactification, where all branes are special Lagrangian, and open strings live at the intersections between pairs of branes. At least if all intersections have the same sign, there are $\langle\gamma_i, \gamma_j\rangle$ of them, and this must also be the number of $U(n_i) - U(n_j)$ bifundamental fields in the gauge theory.

dimension vector $\mathbf{n} = (n_i)$ to describe the D-brane state. An isomorphism of representations is just a gauge transformation.

Such quiver descriptions of D-brane moduli spaces are known to be accurate for fractional D-branes on orbifolds [70]. They also exist for some non-compact Calabi-Yau models (like the conifold) in which D-brane central charges can have almost equal arguments [71, 68]. For a compact Calabi-Yau, however, a quiver gives at best a local description of the moduli space of D-branes near a wall of marginal stability.

As $g_s \to 0$, a bound collection of D-branes can undergo tachyon condensation due to tachyonic modes acquired by open string states between pairs of branes. Indeed, if the bound collection of D-branes is to be stable, it *must* undergo tachyon condensation, "decaying" to a *single*, potentially complicated, D-brane state at very small g_s. It was argued in [57] that near a wall of marginal stability, the Denef stability condition (2.2.1) is equivalent to θ-stability for a quiver or gauge theory, and equivalent to the physical requirement of having tachyonic open string states present.

Categories of branes

Mathematically, D-branes are described by objects in the Fukaya category (in type IIB compactification) or the derived category of coherent sheaves $D^b coh(X)$ (in type IIA compactification).[9] In each case, BPS branes must satisfy a stability condition — respectively, Joyce stability [73] and Π-stability [18] — to ensure that they are stable objects that cannot decay (in a physical type II theory) into independent constituent branes. These stability conditions depend on the vector multiplet moduli t_∞ of the Calabi-Yau compactification, and are equivalent to Denef stability near walls of marginal stability. Moreover, for quiver quantum mechanics, they should be equivalent to θ-stability. To summarize, there is a (still conjectural!) equivalence of stable moduli spaces

$$\begin{aligned}\mathcal{M}_{Fuk}\big(\tilde{\gamma}; \text{Joyce}(t_\infty)\big) \overset{\text{mirror}}{=} \mathcal{M}_{D^b coh}\big(\gamma; \Pi(t_\infty)\big) &= \mathcal{M}_s\big(\gamma = \sum n_i\gamma_i; \boldsymbol{\theta}(t_\infty)\big) \\ &= \mathcal{M}(\text{D-brane bound state of charge } \gamma \text{ at } t_\infty)\,,\end{aligned} \tag{2.3.5}$$

and a corresponding equivalence of Hilbert spaces

$$\mathcal{H}'^{brane}_{BPS}(\gamma; t_\infty) = \mathcal{H}'^{sugra}_{BPS}(\gamma; t_\infty)\,. \tag{2.3.6}$$

[9] There is a large body of literature on this topic; see [72] for an excellent review.

As a final comment, note that there exists a general construction of quivers directly from the categorical description of branes. Suppose that we are in a IIA compactification, so the relevant category is $D^b coh(X)$. Given a collection of branes that form a basis for the associated K-theory on X — *i.e.* branes whose charges γ_i generate the charge lattice Γ — one can form a quiver by associating a node to each such brane, arrows to each Ext^1 group between pairs of branes, and a superpotential computed from the Ext^2 groups. Then quiver representations of dimension vector $\mathbf{n}$ such that $\sum_i n_i\gamma_i = \gamma$ (such a dimension vector can be found for any γ) should describe D-brane states of total charge γ. Unfortunately, if some of the branes in the chosen K-theory basis are not rigid, the resulting quiver can have closed loops (from a node to itself) that are not "obstructed" by the superpotential. In this case, the moduli space of quiver representations is noncompact, and only describes the D-brane moduli space $\mathcal{M}(\gamma)$ locally. As it is not known how to compactify $\mathcal{M}(\gamma)$, it is not clear how to compute the respective $\mathcal{H}'_{BPS}(\gamma)$. A rigid, complete basis for the quiver *can* be found in the situations mentioned above: orbifolds and some non-compact Calabi-Yau's. In some cases, it is possible to consider a sublattice of $\Gamma' \subset \Gamma$ that has a rigid basis of branes, and to obtain compact moduli spaces for $\gamma \in \Gamma'$.

2.4 Invisible walls

In this final section, we examine the "invisible walls" introduced in Section 2.1. We defined these to be walls in moduli space across which the unrefined index $\Omega(\gamma)$ is continuous, but the refined index $\Omega^{ref}(\gamma; y)$ jumps. The basic mechanism for how this happens can be understood in a simple situation where $\mathcal{H}_{BPS}(\gamma)$ admits a description as the cohomology of a brane moduli space $\mathcal{M}(\gamma)$. As t_∞ (say) crosses an invisible wall, $\mathcal{M}(\gamma)$ can develop a singularity and undergo a topology-changing transition, so that the Poincaré polynomial of $\mathcal{M}$ changes while the Euler characteristic does not.

In the vector multiplet moduli space $\mathcal{M}_V$, one tempting place to look for such invisible walls is in internal rearrangements of multi-center black holes that were first considered in [20] (Section 5.2.3 therein). The basic idea is that as t_∞ varies the components of a multi-center state can change their binding structure, and presumably change the spin structure of the overall configuration, without ever undergoing a marginal stability transition. We focus here on this example — and find, amazingly, that multiple factors conspire to assure

that the refined index remains unchanged.

Multi-center rearrangements

The simplest scenario, involving a 3-center bound state of total charge $\gamma = \gamma_1 + \gamma_2 + \gamma_3$ with all component charges primitive, is depicted in Figure 2.5. For one value of moduli $t_\infty = t_0$, an attractor flow first encounters a $\arg Z(\gamma_2) = \arg Z(\gamma_1 + \gamma_3)$ wall. If the flow splits, it eventually forms attractor flow tree (A). If it crosses this wall without splitting, it forms attractor flow tree (B). However, for a slightly different value of moduli $t_\infty = t_1$, the flow hits a $\arg Z(\gamma_3) = \arg Z(\gamma_1 + \gamma_2)$ wall first and must split there to form attractor flow tree (C). *Note that there is no marginal stability wall between t_0 and t_1.*

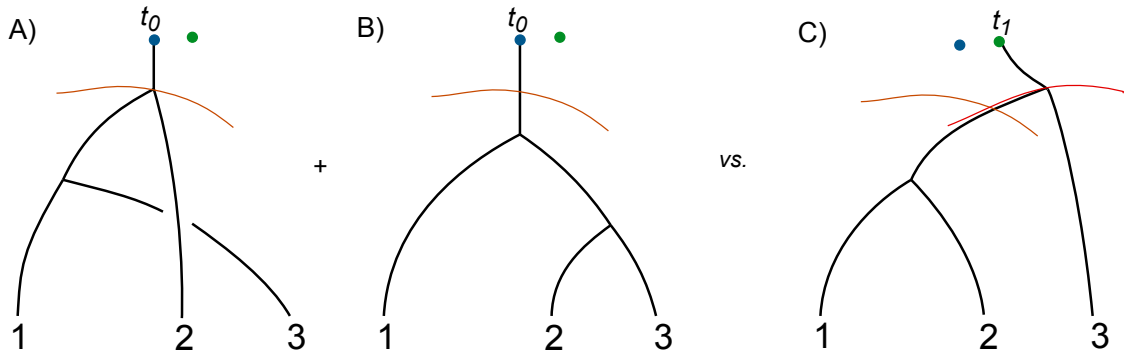

Figure 2.5: A three-center rearrangement.

This scenario may seem somewhat contrived, but it can actually happen in a physical context: the example given in [20] involves a 3-centered $D6 - D6 - \overline{D6}$ bound state (where the two $D6$'s have nontrivial worldvolume flux). Generally, a necessary condition for this transition is that the three quantities

$$a = \langle \gamma_2, \gamma_3 \rangle \qquad b = \langle \gamma_3, \gamma_1 \rangle \qquad c = \langle \gamma_1, \gamma_2 \rangle \tag{2.4.1}$$

all have the same sign. Assuming (WLOG) they are all positive, it is also necessary that

$$a > b > c\,. \tag{2.4.2}$$

Since the transition does not involve crossing a wall of marginal stability, the unrefined index $\Omega(\gamma)$ should not change. To see that this is indeed the case, one can use repeated

applications of the primitive wall-crossing formula (2.2.6). Since $\mathcal{H}(\gamma;t_0) = \mathcal{H}^{(A)}(\gamma;t_0) \oplus \mathcal{H}^{(B)}(\gamma;t_0)$, the index at t_0 is

$$\begin{aligned}\Omega(\gamma;t_0) &= (-1)^{a-c+b}(a-c)b\,\Omega(\gamma_1)\Omega(\gamma_2)\Omega(\gamma_3) + (-1)^{c-b+a}(c-b)a\,\Omega(\gamma_1)\Omega(\gamma_2)\Omega(\gamma_3) \\ &= (-1)^{a+b+c}\big[(a-c)b + (c-b)a\big]\,\Omega(\gamma_1)\Omega(\gamma_2)\Omega(\gamma_3)\,. \end{aligned} \tag{2.4.3}$$

The index at t_1 is similarly given by

$$\Omega(\gamma;t_1) = (-1)^{a-b+c}(a-b)c\,\Omega(\gamma_1)\Omega(\gamma_2)\Omega(\gamma_3)\,, \tag{2.4.4}$$

and $\Omega(\gamma;t_0) = \Omega(\gamma;t_1)$ results from the simple fact that $(a-c)b + (c-b)a = (a-b)c$.

In the refined case, we can similarly iterate the refined primitive wall-crossing formula (2.2.7) to find that

$$\begin{aligned}&\Omega^{ref}(\gamma;t_0;y) - \Omega^{ref}(\gamma;t_1;y) \\ &\quad = \big([a-c]_{-y}[b]_{-y} + [c-b]_{-y}[a]_{-y} - [a-b]_{-y}[c]_{-y}\big)\,\Omega^{ref}(\gamma_1;y)\Omega^{ref}(\gamma_2;y)\Omega^{ref}(\gamma_3;y)\,. \end{aligned} \tag{2.4.5}$$

It is a surprising fact that the quantity in parentheses actually vanishes, due to an algebraic identity of quantum dimensions. Therefore, in this case, there is no change in the refined index either: although the internal configuration of the bound state is rearranged, the total structure of the spin is unmodified!

Although the scenario just described is a rather simple example, it forms the basis for an argument that no invisible walls exist for rearrangements of *any* multi-center states, at least when the component black holes have primitive charges. Observe first that if there *had* existed an invisible wall in the 3-center rearrangement, it would correspond to all moduli t_{inv} such that the attractor flow for charge γ from t_{inv} would hit the codimension-2 locus Y where

$$\arg Z(\gamma_1) = \arg Z(\gamma_2) = \arg Z(\gamma_3)\,. \tag{2.4.6}$$

This is shown schematically in Figure 2.6. The (non-generic!) attractor flow tree from moduli t_∞ on this putative wall undergoes a triple split, serving as a transition between trees (A) and (B) and tree (C).

Now imagine a general (primitive) multi-center rearrangement, where for some value of starting moduli $t_\infty = t_0$ a certain set $\mathcal{T}_0$ of tree topologies are possible; and for some other value $t_\infty = t_1$ some other set $\mathcal{T}_1$ of topologies are achieved. A path in moduli space from t_0 to t_1 encounters putative invisible walls at some set of moduli $t^{(1)}, t^{(2)}, t^{(3)}, ...$ whose

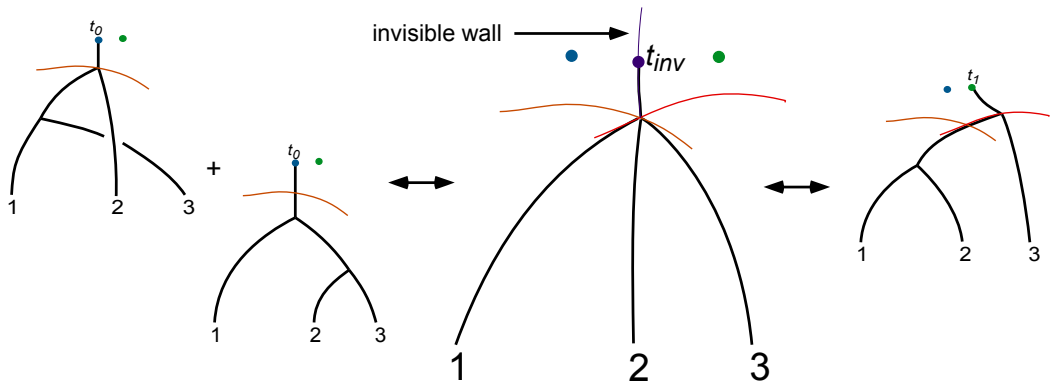

Figure 2.6: An invisible wall located at a three-way split.

attractor flows hit points where the arguments of three or more central charges align — at these points topologies in the set $\mathcal{T}_0$ can merge and split, so they eventually transition to the topologies of $\mathcal{T}_1$. However, since a locus where n central charges align is generically of real codimension $(n-1)$ in $\mathcal{M}_V$, it should be possible to adjust the path from t_0 to t_1 such that all the putative invisible walls it encounters correspond to the arguments of just three central charges aligning. Then the transition between sets $\mathcal{T}_0$ and $\mathcal{T}_1$ factors completely into a sequence of 3-center transitions that locally look just like the one in Figure 2.6. Since the refined index does not change in the 3-center case, it cannot change in the multi-center case either.

Non-primitive rearrangements

The above analysis can be extended to non-primitive rearrangements, though the relevant scenarios quickly increase in complexity. For example, consider the formation of a bound state with total charge

$$\gamma = \gamma_1 + \gamma_2 + 2\gamma_3 \,. \tag{2.4.7}$$

In addition to the three basic tree topologies corresponding to Figure 2.5, there are three additional options as shown below in Figure 2.7. In a physical scenario like the $D6$–$D6$–$\overline{D6}$ bound states of [20], only a subset of the potential tree topologies will be realized. Exactly which ones appear depends on the relative magnitudes of $a = \langle\gamma_2, \gamma_3\rangle$, $b = \langle\gamma_3, \gamma_1\rangle$, and $c = \langle\gamma_1, \gamma_2\rangle$. Unlike the primitive case, where (2.4.2) was the only nontrivial possibility, there are *multiple* parameter regimes for which topology transitions can take place.

All these regimes, and even more complicated non-primitive examples, are analyzed in [4]. The astonishing result is that the refined index *never* changes from one side of a putative invisible wall to the other. This suggests a

Conjecture: In the vector multiplet moduli space, the refined index can only jump at true walls of marginal stability.

In other words, we expect that continuity of the unrefined index implies continuity of the refined index. This conjecture is pleasingly consistent with the general quantum/motivic wall-crossing formula that will be discussed in Chapter 4. Indeed, if motivic Donaldson-Thomas invariants are a completely accurate mathematical realization of refined physical BPS invariants — and so far we have no reason to think otherwise — then motivic wall crossing *predicts* the absence of invisible walls.

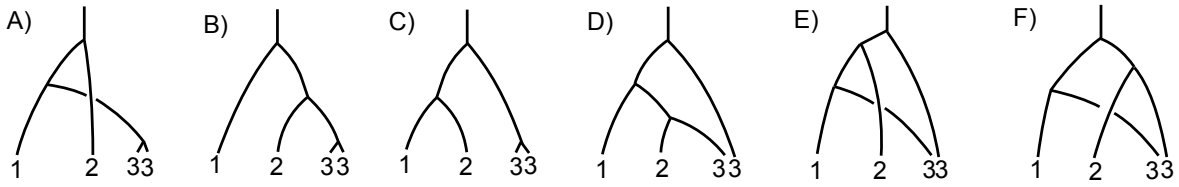

Figure 2.7: Possible multi-center tree topologies in the simplest non-primitive case. Here we draw two separate γ_3 attractor points just to distinguish flows of charge γ_3 and $2\gamma_3$; physically, they are the same point in moduli space.

As an explicit illustration of a non-primitive rearrangement, let us take $a > b > c > 0$, as in (2.4.2). Then physical considerations predict that (A) and (D) will be realized on one side of the putative invisible wall, while (B) and (C) will be realized on the other. The refined semi-primitive wall-crossing formula (2.2.13) predicts in general that

$$\Omega^{ref}(\gamma+2\eta;y) = \Omega^{ref}(\gamma;y)\left(\frac{1}{2}[I]_y^2\Omega^{ref}(\eta;y)^2 - \frac{1}{2}[I]_{y^2}\Omega^{ref}(\eta;y^2) - [2I]_y\Omega^{ref}(2\eta;y)\right), \tag{2.4.8}$$

where $I = |\langle\gamma,\eta\rangle|$, and we have suppressed the dependence on moduli $t_\pm$ in Ω^{ref}. Using this formula to work out the total degeneracy $\Omega^{ref}(\gamma_1+\gamma_2+2\gamma_3)$ for each tree topology, we find that $\Omega_A^{ref} + \Omega_D^{ref} = \Omega_B^{ref} + \Omega_C^{ref}$ can only hold in general if each of the following three

relations is satisfied:

$$[2a-c]_y[2b]_y = [c]_y[2a-2b]_y + [2b-c]_y[2a]_y \tag{2.4.9a}$$

$$[2a-c]_y[b]_{y^2} = [c]_y[a-b]_{y^2} + [2b-c]_y[a]_{y^2} \tag{2.4.9b}$$

$$[2a-c]_y[b]_y^2 + 2[a-b]_y[a-c]_y[b]_y = [c]_y[a-b]_y^2 + [2b-c]_y[a]_y^2\,. \tag{2.4.9c}$$

These are all identities for the quantum dimension.

Chapter 3

Refined Wall Crossing via Melting Crystals

In this chapter, we specialize to type IIA "compactifications" on the resolved conifold $X = \mathcal{O}(-1) \oplus \mathcal{O}(-1) \to \mathbb{P}^1$. This is a noncompact Calabi-Yau, but can be thought of as the local (or decompactification) limit of a compact Calabi-Yau into which the conifold is embedded. In this decompactification limit, all Kähler classes except the class of a distinguished $\mathbb{P}^1$ become large. The resolved conifold is a *rigid* Calabi-Yau, in the sense that it has no complex structure deformations. Thus $\mathcal{M}_H$ is trivial and the refined BPS index (2.1.30) is a well-defined function on the Kähler moduli space $\mathcal{M}_V$. (Noncompact toric Calabi-Yau's generally have this property.)

The conifold provides an excellent example of the wall-crossing formulas of Section 2.2, and the relation between BPS indices and standard topological string invariants. In Section 3.1, following [31], we describe the picture of walls, chambers, and unrefined generating functions for the conifold. We then generalize this picture to our refined invariants, and use refined wall crossing to produce refined generating functions in all chambers (following our work in [1]).

The latter part of this chapter is devoted to the study of melting crystal models for conifold invariants and their connection to refined and unrefined wall crossing. The idea that melting crystals can encode topological invariants of Calabi-Yau threefolds (and describe topological strings in such backgrounds) goes back to [25] and [74]. There, the topological vertex, the building block of Gromov-Witten/Gopakumar-Vafa/Donaldson-Thomas parti-

tion functions for noncompact toric Calabi-Yau's, is reinterpreted as the generating function of *plane partitions* — or cubic crystals melting in the corner of a room. However, another set of crystal models, based more closely on the toric web of a noncompact Calabi-Yau,is also discussed in this literature. For a conifold, this "other model" consists of *pyramid partitions*.

More recently, B. Szendröi [64] used pyramid partitions to describe the representations of the noncommutative path algebra generated by the conifold quiver (or by a noncommutative resolution of the conifold). This path algebra defined "noncommutative Donaldson-Thomas theory." The generating function for pyramid partitions computes the noncommutative Donaldson-Thomas partition function. Jafferis and Chaung [75] then generalized this approach to the generating function of D6-D2-D0 bound states in all chambers for the resolved conifold: in each chamber, the meltings of a pyramid crystal with different boundary conditions determine the corresponding generating function.

In Section 3.3, we very briefly describe the approach used by [75] to identify crystal boundary conditions with stability conditions. It requires the study of quiver representations at different choices of θ-stability. In Section 3.3, we then review a mathematical proof by B. Young [76] that crystals with differing boundary conditions actually reproduce the generating functions for the resolved conifold, and argue that an algorithm called *dimer shuffling* provides a combinatorial realization of wall crossing. Moreover, we use dimer shuffling/wall crossing to relate a limit of pyramid partitions to the topological vertex. Finally, in Section 3.4, we show that the everything can be refined. By splitting pyramid partitions on diagonals and thereby modifying the weights assigned to their atoms, we obtain refined partition functions in all chambers; and we related refined pyramid partitions to the refined topological vertex. Sections 3.3 and 3.4 are based on our work in [1].

Although we focus mainly on the example of the conifold here, many results *should* generalize to more complicated noncompact Calabi-Yau manifolds. Indeed, since [1] was published, some partial generalizations have appeared in [32, 33].

3.1 Wall crossing for the conifold

The picture of walls and chambers for the resolved conifold $X = \mathcal{O}(-1) \oplus \mathcal{O}(-1) \to \mathbb{P}^1$ was developed in [31]. In order to analyze wall crossing this non-compact Calabi-Yau properly, one must embed it in a compact global geometry and then look at the subset of walls and BPS states that survive in the local limit — the limit where all Kähler classes except that of the $\mathbb{P}^1$ become large.

To be more specific, let β be the generator of $H^4(X;\mathbb{Z})$, dual to the rigid cycle on $\mathbb{P}^1 \in X$. Then, the Kähler parameter in the compact geometry is taken to be

$$t = z\,\mathcal{P} + \Lambda e^{i\varphi}\,\mathcal{P}' \ \in H^2(X,\mathbb{C})\,, \tag{3.1.1}$$

where $\mathcal{P}\cdot\beta = 1$, $\mathcal{P}'\cdot\beta = 0$, and $(\mathcal{P}')^3 > 0$. Here, z is a complex number parametrizing $B + iJ$ on $\mathbb{P}^1$, and $\Lambda e^{i\varphi}$ is a complex number parametrizing all the other Kähler classes, whose magnitude Λ one takes to be very large. In the limit $\Lambda \to \infty$, the phase φ still survives as a finite parameter, and effectively enlarges the Kähler parameter space of the resolved conifold to have real dimension *three*.

In the notation of [31], charge of a bound state of a D6 brane, M D2 branes, and N D0 branes can be written as a cohomology class

$$\gamma_{1,M,N} = 1 - M\beta + N dV \ \in H^{even}(X;\mathbb{Z}), \tag{3.1.2}$$

where dV is the volume element on X, normalized so that $\int_X dV = 1$ (in any compact approximation). In the local limit $\Lambda \to \infty$, the central charge of a D6 brane with any number of bound $D2$ and $D0$ branes becomes

$$Z(1 - \ldots) \sim \Lambda^3 e^{3i\varphi}\,, \tag{3.1.3}$$

while the central charge of a D2-D0 bound state (with no D6) is

$$Z(-M\beta + N dV) = -Mz - N\,. \tag{3.1.4}$$

Thus the parameter φ can also be interpreted as the phase of the central charge of the D6 brane. It is fairly easy to see that in the local limit

- The only single-center (single attractor flow) state is a pure D6.

- The only possible walls of marginal stability correspond to primitive or semi-primitive splits

$$1 - M\beta + NdV \to (1 - M'\beta + N'dV) + (M''\beta + N''dV)\,. \tag{3.1.5}$$

  In particular, no D6-$\overline{\text{D6}}$ bound states ever form.

As φ is varied while keeping z constant, what effectively happens is that the central charge of a D6 brane sweeps across moduli space, binding MD2+ND0 fragments whenever walls of marginal stability

$$\arg e^{3i\varphi} = \arg(-Mz - N) \tag{3.1.6}$$

are encountered.

Since the fragments $-M\beta + nDV$ undergo no wall crossings throughout the local-limit moduli space, one can obtain their unrefined indices from the Gopakumar-Vafa invariants for the conifold [11, 12]:

$$\begin{aligned} \Omega(\pm\beta + NdV) &= 1\,, \\ \Omega(NdV) &= -2\,, \\ \Omega(-M\beta + NdV) &= 0 \quad \text{otherwise}\,. \end{aligned} \tag{3.1.7}$$

This results in the picture of walls and chambers shown in Figure 3.1, covering a large section of moduli space. There is a core region $\tilde{C}_0$, corresponding to Kähler moduli near the attractor point for the D6 brane, where only the pure D6 brane is stable. Varying φ away from this region, one encounters first a D2+D0 wall, then a D2+2D0 wall, then a D2+3D0 wall, etc.; at each transition, the D6 brane binds with an arbitrary number of D2+ND0 particles, *à la* semi-primitive wall crossing. After crossing all D2+ND0 walls, at finite distance in moduli space, one encounters the D0 wall, where any number of D0 particles bind to the D6. Then $\overline{\text{D2}} + ND0$ particles begin to bind until, after crossing a $\overline{\text{D2}} + D0$ wall, one ends up in the Szendröi region of moduli space.

Generating functions

In the core region of moduli space, the partition function of D6-D2-D0 bound states

$$\mathcal{Z}(q, Q; t_\infty) = \sum_{M,N\in\mathbb{Z}} \Omega(1 - M\beta + NdV; t_\infty)(-q)^N Q^M \tag{3.1.8}$$

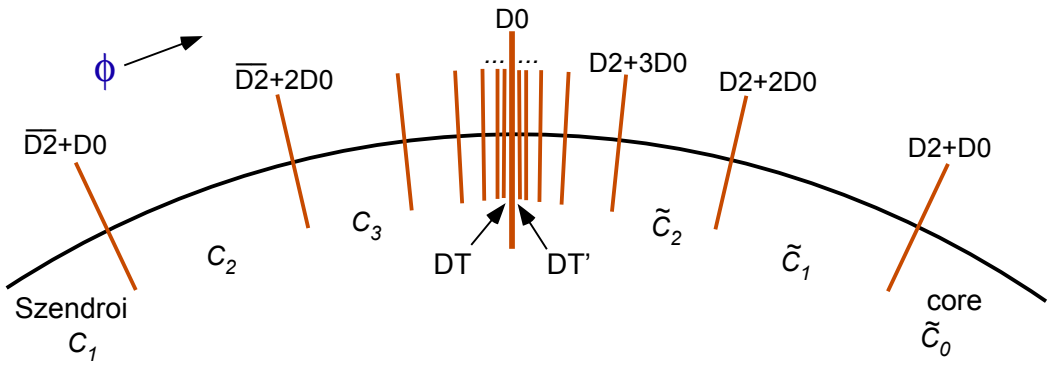

Figure 3.1: Walls and chambers for the refined conifold.

simply takes the value $\mathcal{Z}(q,Q;\tilde{C}_0)=1$. By the semi-primitive wall-crossing formula (2.2.14),[1] the partition function in chamber $\tilde{C}_n$ is then

$$\mathcal{Z}(q,Q;\tilde{C}_n)=\prod_{j=1}^{N}(1-q^jQ)^j\,, \tag{3.1.9}$$

which converges to the reduced Donaldson-Thomas partition function immediately before the D0 wall,

$$\mathcal{Z}(q,Q;\tilde{C}_\infty)=\mathcal{Z}'_{DT}(q,Q)=\prod_{j=1}^{\infty}(1-q^jQ)^j\,. \tag{3.1.10}$$

On the other side of the wall, the binding of a gas of D0's (and 2D0's, 3D0's, etc.) multiplies the partition function by the MacMahon function, resulting in the unreduced Donaldson-Thomas partition function

$$\mathcal{Z}(q,Q;C_\infty)=\mathcal{Z}_{DT}(q,Q)=M(q)^2\prod_{j=1}^{\infty}(1-q^jQ)^j\,. \tag{3.1.11}$$

This is a general phenomenon: when crossing the D6-D0 wall, which exists generically in the large-volume moduli space of Calabi-Yau's, the D6-D2-D0 partition function acquires a factor of $M(q)^{\chi(X)}$.

As one progresses to the Szendöi region, the partition function becomes

$$\mathcal{Z}(q,Q;C_n)=M(q)^2\prod_{j=1}^{\infty}(1-q^jQ)^j\prod_{k=N}^{\infty}(1-q^kQ^{-1})^k\,. \tag{3.1.12}$$

[1]Note that the D2-D0 states are fermionic, whereas the D0 states are bosonic. Thus, the wall-crossing formula at D2-D0 walls tends to be much simpler than at the D0 wall.

In the Szendröi region itself, this finally becomes Szendröi's "noncommutative Donaldson-Thomas" partition function [64]

$$\mathcal{Z}(q,Q;C_1) = \mathcal{Z}_{Sz}(q,Q) = M(q)^2 \prod_{j=1}^{\infty}(1-q^jQ)^j \prod_{k=1}^{\infty}(1-q^kQ^{-1})^k \,. \tag{3.1.13}$$

Refined generating functions

It is not too difficult to generalize the above story, summarized from [31], to our unrefined invariants. There do not seem to be any invisible walls in the region of moduli space depicted in Figure 3.1, so we only need worry about marginal stability transitions. Furthermore, it is clear from an analysis of the moduli space of D0 and D2-D0 branes on the conifold (or from refined Gopakumar-Vafa invariants [23, 26]) that D2+ND0 states belong to fermionic hypermultiplets and ND0 states belong to bosonic vector multiplets — "bosonic" and "fermionic" referring to their statistics in the internal Hilbert space $\mathcal{H}'$, with center-of-mass degrees of freedom factored out. Therefore (*cf.* (2.1.32)-(2.1.33)),

$$\begin{aligned} \Omega^{ref}(\pm\beta + NdV; y) &= 1\,, \\ \Omega^{ref}(NdV; y) &= -y - y^{-1}\,, \\ \Omega^{ref}(-M\beta + NdV; y) &= 0 \quad \text{otherwise}\,. \end{aligned} \tag{3.1.14}$$

As in Section 2.1, let us define the refined generating function of D6-D2-D0 states as

$$\mathcal{Z}(q,Q,y;t_\infty) = \sum_{M,N\in\mathbb{Z}} \Omega^{ref}(1-M\beta+NdV;t_\infty;y)(-q)^N Q^M \,. \tag{3.1.15}$$

It is also convenient to change variables from y and q to q_1 and q_2, which are more standard in the literature on topological string invariants, *cf.* [22, 23, 26, 29]:

$$q_1 = qy\,, \qquad q_2 = \frac{q}{y}\,. \tag{3.1.16}$$

Then we have

$$\mathcal{Z}(q_1,q_2,Q;\tilde{C}_0) = 1\,, \tag{3.1.17}$$

$$\mathcal{Z}(q_1,q_2,Q;\tilde{C}_n) = \prod_{\substack{i,j\geq 1\\ i+j\leq N+1}} \left(1+q_1^{i-\frac{1}{2}}q_2^{j-\frac{1}{2}}Q\right), \tag{3.1.18}$$

$$\mathcal{Z}(q_1,q_2,Q;\tilde{C}_\infty) = \prod_{i,j\geq 1} \left(1+q_1^{i-\frac{1}{2}}q_2^{j-\frac{1}{2}}Q\right) = \mathcal{Z}_{DT}^{ref\,\prime}(q_1,q_2,Q)\,, \tag{3.1.19}$$

$$\mathcal{Z}(q_1,q_2,Q;C_\infty) = M(q_1,q_2)^2 \prod_{i,j\geq 1} \left(1+q_1^{i-\frac{1}{2}}q_2^{j-\frac{1}{2}}Q\right) = \mathcal{Z}_{DT}^{ref}(q_1,q_2,Q)\,, \tag{3.1.20}$$

$$\mathcal{Z}(q_1,q_2,Q;C_N) = M(q_1,q_2)^2 \prod_{i,j\geq 1} \left(1+q_1^{i-\frac{1}{2}}q_2^{j-\frac{1}{2}}Q\right) \prod_{\substack{k,l\geq 1\\ k+l\geq N}} \left(1+q_1^{k-\frac{1}{2}}q_2^{l-\frac{1}{2}}Q^{-1}\right), \tag{3.1.21}$$

$$\mathcal{Z}(q_1,q_2,Q;C_1) = M(q_1,q_2)^2 \prod_{i,j\geq 1} \left(1+q_1^{i-\frac{1}{2}}q_2^{j-\frac{1}{2}}Q\right)\left(1+q_1^{i-\frac{1}{2}}q_2^{j-\frac{1}{2}}Q^{-1}\right) = \mathcal{Z}_{Sz}^{ref}(q_1,q_2,Q)\,. \tag{3.1.22}$$

These generating functions all follow by applying the semi-primitive wall-crossing formula (2.2.13) at each D2-D0, D0, and $\overline{\text{D2}}$-D0 wall, starting from the core region $\tilde{C}_0$. Of course, in the core region both refined and unrefined generating functions are trivial, since the only state in the spectrum is the pure D6.

Observe that on either side of the D0 wall the refined generating function reproduces the refined Donaldson-Thomas/Gopakumar-Vafa partition function for the resolved conifold, as calculated with the refined topological vertex [26]. This should be no great surprise: the stability conditions near the D0 wall are such that all D2-D0 fragments can bind to the D6, but no $\overline{\text{D2}} - D0$ fragments can bind, which appropriately describes the ideal sheaves in Donaldson-Thomas theory [65]. The extra spin content of the present BPS invariants is equivalent to the extra $SU(2)$ Lefschetz action used in defining refined Donaldson-Thomas invariants.

The two sides of the D0 wall are related by a *refined MacMahon function*, which we have normalized symmetrically here to be $M(q_1,q_2) = \prod_{i,j\geq 1}\left(1-q_1^{i-\frac{1}{2}}q_2^{j-\frac{1}{2}}\right)$. In general, when studying BPS invariants one encounters a family of refinements

$$M_\delta(q_1,q_2) = \prod_{i,j\geq 1}\left(1-q_1^{i-\frac{1}{2}+\frac{\delta}{2}}q_2^{j-\frac{1}{2}-\frac{\delta}{2}}\right), \tag{3.1.23}$$

which all reduce to the ordinary MacMahon function $M(q)$ in the limit $y\to 1$. (In the "opposite" opposite $y\to -1$, the functions (3.1.23) specialize to $M(-q)$, which describes the contribution of the 0-dimensional subschemes to the $\widehat{\text{DT}}$-invariants of [77].)

In the Szendröi chamber C_1, the generating function (3.1.22) refines Szendröi's partition function for noncommutative Donaldson-Thomas theory on the conifold. The answer here, derived via wall-crossing, agrees with a more rigorous mathematical calculation for an appropriately refined noncommutative Donaldson-Thomas partition function.[2]

3.2 Crystals and quivers

In the final two sections of this chapter, we will discuss refined and unrefined crystal-melting models and "combinatorial wall crossing" for the D6-D2-D0 BPS generating functions of the refined conifold. In order to maintain continuity of ideas, we presently take a moment to very briefly review the general connection between crystal models, quivers, and BPS states.

Crystal-melting models were first used to describe BPS states in the Gromov-Witten/ Donaldson-Thomas chamber of noncompact toric Calabi-Yau's in [25], where it was realized that the topological vertex [24] was a generating function of three-dimensional plane partitions (or boxes stacked in the corner of a room). In terms of Donaldson-Thomas theory, plane partitions describe fixed points under a torus action in the moduli space of ideal sheaves on $\mathbb{C}^3$ [9, 10]. In the topological vertex formalism, the full toric Calabi-Yau X is glued together from copies of $\mathbb{C}^3$, and the moduli space $\mathcal{M}$ of ideal sheaves on X is glued together from moduli spaces on $\mathbb{C}^3$. The Euler characteristic or cohomology of $\mathcal{M}$ (hence Donaldson-Thomas invariants) can then be related to the plane partitions that describe local fixed points, by standard localization theorems (*cf.* [78]). The topological vertex was generalized to a *refined* vertex (with refined plane partitions) in [26], to describe refined Gromov-Witten/Donaldson-Thomas invariants.

Szendröi [64] recently described a very different melting crystal model for the noncommutative Donaldson-Thomas chamber C_1 of the conifold. In this special, extreme chamber of $\mathcal{M}_V$, the classical moduli spaces $\mathcal{M}(\gamma)$ of BPS states (*i.e.* the moduli spaces whose "quantization" give $\mathcal{H}_{BPS}(\gamma)$) correspond to *cyclic* representations of the conifold quiver algebra. All the vector spaces V_i (*cf.* Section 2.3) of a cyclic representation of a quiver are

[2]We thank B. Szendröi for discussions on this topic.

generated by a single basis element $\mathbf{e}$ in the vector space $V_{i'}$ of some distinguished vertex i'. The resulting moduli spaces $\mathcal{M}\gamma$ have a toric action, whose fixed points again describe partitions, or molten crystal configurations. However, the relevant pyramid crystal, shown on the left-hand side of Figure 3.4 on page 50, looks very different from the plane partitions of the topological vertex. Such Szendröi-chamber melting crystal models were generalized to other noncompact toric Calabi-Yau's in [79] (see also [80]), but they have not yet been refined. (We will present a refinement in Section 3.4.)

Of course, there are many more chambers of moduli space, and one would like to have a crystal model in each one. Jafferis and Chuang [75] realized how to accomplish this by relating cyclic quiver representations — which lead directly to crystals — with θ-stable representations. In the case of noncompact toric Calabi-Yau's with a good quiver description, the moduli spaces $\mathcal{M}(\gamma; t)$ at different moduli $t \in \mathcal{M}_V$ correspond to stable quiver representations with different $\boldsymbol{\theta}$ parameters. Jafferis and Chaung showed that by appropriately choosing a different basis of coherent sheaves to generate the quiver in each chamber $\mathcal{M}_V$, θ-stability could always reduce to cyclicity.

As an example of this construction, consider the conifold in the Szendröi chamber C_1. The appropriate representation of the conifold quiver in this chamber is shown in Figure 3.2. The basis of coherent sheaves consists of the D6-brane $\mathcal{O}_X[1]$, the $\overline{\text{D2}}$+D0 brane $\mathcal{O}_{\mathbb{P}^1}(-2)[1]$, and the D2 brane $\mathcal{O}_{\mathbb{P}^1}(-1)$. In the Szendröi chamber, the θ-parameters for the three corresponding vertices satisfy $\theta_1 > 0$, $\theta_2 < 0$, and $\theta_3 < 0$, respectively. The stable representations with dimension vector $\mathbf{n} = (1, N, M+N)$, corresponding to bound states of D6+MD2+ND0 branes, then become completely equivalent to the cyclic representations generated by the D6 vertex.

It is also fairly easy to see in this simple example how pyramid partitions (meltings of the C_1 crystal in Figure 3.4) are identified with representations corresponding to fixed points of the full moduli space of stable/cyclic representations. Consider a set of atoms that have been removed in a melting configuration, such as in Figure 3.3. Suppose there are N white atoms and $M + N$ black atoms. This corresponds to a quiver representation of dimension $\mathbf{n} = (\dim V_1, \dim V_2, \dim V_3) = (1, N, M + N)$, where each white atom is associated to a basis element of V_2 and each black atom to a basis element of V_3. To determine the homomorphisms represented by the arrows A_1, A_2, B_1, B_2, draw four arrows from each white atom to the layer of black atoms below it (and vice verse) as shown on the

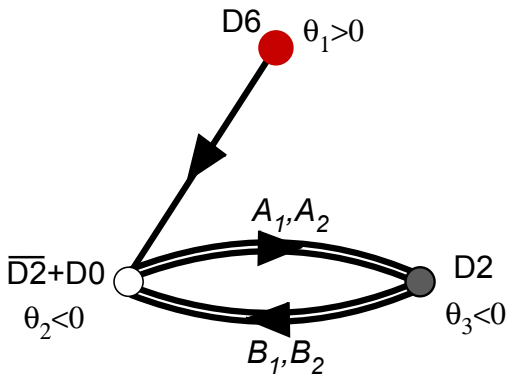

Figure 3.2: The conifold quiver for the C_1 chamber, with charges of nodes and θ-parameters as indicated. The superpotential is $W = \mathrm{Tr}(A_1B_1A_2B_2 - A_1B_2A_2B_1)$.

right side of Figure 3.3. Each A_1 arrow connecting two atoms in the finite removed/melted set corresponds to a '1' entry in the homomorphism matrix representing A_1, a mapping between the basis elements associated to the atoms. All other entries in the matrix A_1 are set to zero. Likewise, A_2, B_1, and B_2 are constructed, completing the representation. It is argued in [64] that *every fixed point* in the moduli space of cyclic representations is identified uniquely with a melting configuration like this. Note that the "distinguished" vector that generates these cyclic representations is basis of the one-dimensional space V_1, which maps to the basis element of V_2 corresponding to the single white atom at the top of the crystal (present in every crystal melting), and maps subsequently to the rest of the melted atoms. The superpotential conditions $dW = 0$ for a good quiver representation simply state that different paths connecting a black or white atom to any atom three layers under it are equivalent.

3.3 Pyramid crystals and wall crossing

We now consider the (unrefined) melting crystal descriptions of the conifold partition functions in chambers $\tilde{C}_n$ and $\tilde{C}_n$ more carefully. After summarizing the basic result from [75] in all chambers, we review Young's mathematical proof that the infinite crystals corresponding to chambers C_n actually give the right answers. Moreover, we argue that *dimer shuffling*, to be defined below, provides a combinatorial realization of wall crossing that, in the limit $n \to \infty$ (the DT chamber), causes pyramid partitions to reduce to the usual

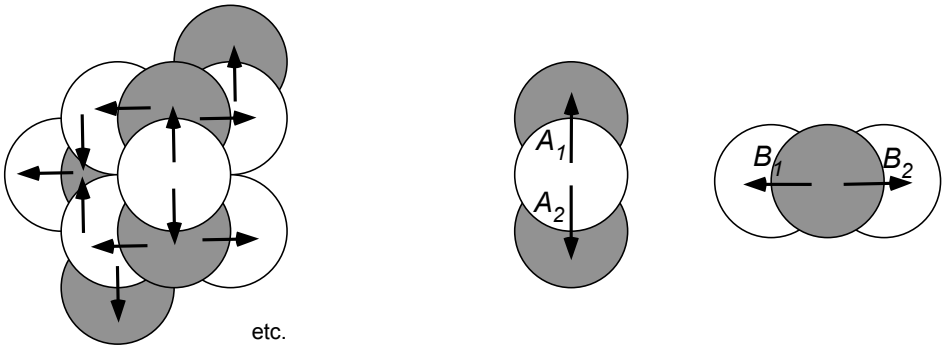

Figure 3.3: A set of atoms melted from the C_1 crystal (right); and assignment of arrows A_1, A_2, B_1, B_2 to atoms (left).

topological vertex model for the conifold.

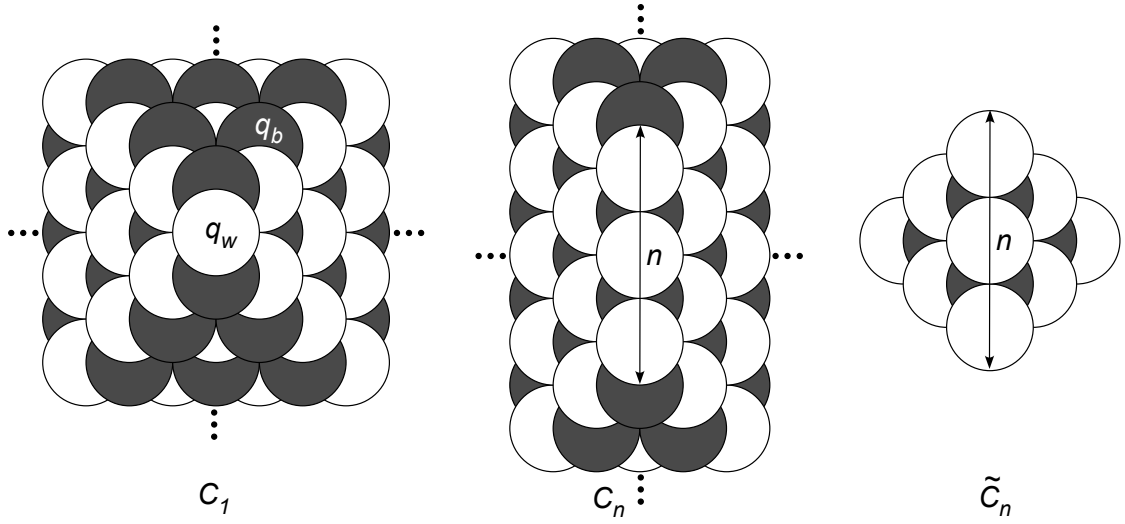

Figure 3.4: The "empty room configurations" for the crystals that count BPS states in chambers C_n and $\tilde{C}_n$.

In the chamber C_n, the unrefined generating function of BPS states is obtained by counting the melting configurations of an infinite pyramid-shaped crystal whose top row of atoms has length n (sometimes also called an empty room configuration, or ERC, of length n) [64, 75]. As shown in Figure 3.4, this crystal has two different types of atoms, corresponding to the two vertices of the Klebanov-Witten quiver. The top edge of the pyramid always consists of n white atoms. The remainder of the pyramid is then constructed by placing two black atoms underneath each white atom, oriented vertically, and two white

atoms underneath each black one, oriented horizontally.[3] In order for an atom to be removed during crystal melting, all atoms lying above it must be removed as well. The partition function is defined as a sum over all melting configurations (*i.e.* pyramid partitions) π,

$$Z(q_w, q_b; C_n) = \sum_{\pi} q_w^{w_w(\pi)} q_b^{w_b(\pi)} \,, \tag{3.3.1}$$

where $w_w(\pi)$ and $w_b(\pi)$, respectively, are the numbers of white and black atoms removed. It was proven in [76] that this agrees with the partition function (3.1.12),

$$Z(q_w, q_b; C_n) = Z(q, Q; C_n) = M(q)^2 \prod_{j=1}^{\infty} (1 - q^j Q)^j \prod_{k=n}^{\infty} (1 - q^k Q^{-1})^k \,, \tag{3.3.2}$$

provided that one makes an n-dependent identification as in [75],

$$C_n : \qquad q_w = -q^n Q^{-1} \,, \qquad q_b = -q^{-(n-1)} Q \,. \tag{3.3.3}$$

Similarly, it was argued in [75] that to obtain the unrefined partition function in the chamber $\tilde{C}_n$ one must sum over the melting configurations of a *finite* crystal configuration of length n, also shown in Figure 3.4. Then

$$Z(q, Q; \tilde{C}_n) = \prod_{j=1}^{n} (1 - q^j Q)^j = \sum_{\pi} q_w^{w_w(\pi)} q_b^{w_b(\pi)} \tag{3.3.4}$$

if one identifies

$$\tilde{C}_n : \qquad q_w = -q^n Q \,, \qquad q_b = -q^{-(n+1)} Q^{-1} \,. \tag{3.3.5}$$

To proceed further, let us translate the above partition functions into the language of dimers. The partitions of a length-n pyramid correspond bijectively to the states of a dimer model on a square lattice with prescribed asymptotic boundary conditions. (We will refer to these states as partitions as well.) An intuitive way to visualize the correspondence (see also [76]) is to actually draw dimers on the black and white atoms, as in Figure 3.5. Then the dimer state corresponding to a given crystal automatically appears when viewing the crystal from above.

As in [76], we have included an extra decoration on the lattices in these figures: lattice points are colored with alternating black and white dots. This canonical decoration carries no extra information, but is very useful in describing weights and wall crossing. We will

[3] In nature, such a crystal structure, very similar to that of diamond, occurs in moissanite (silicon carbide) and the semiconductor gallium arsenide.

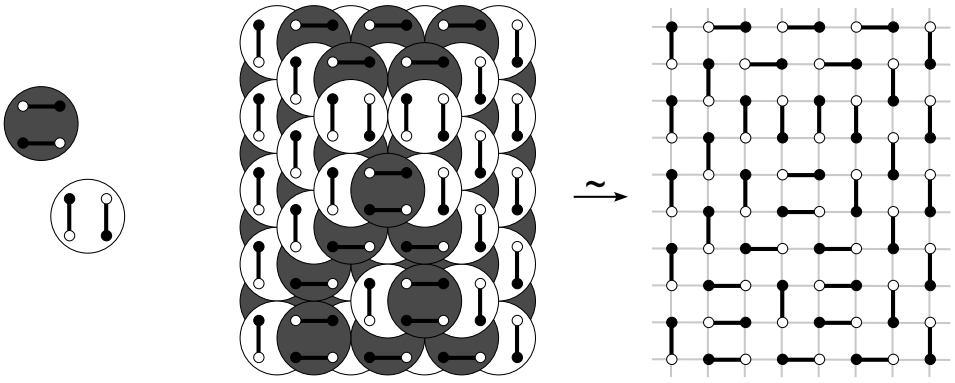

Figure 3.5: The relation between pyramid partitions and dimer states, illustrated for $n = 2$.

Figure 3.6: Even and odd boxes of dimers.

also call squares in the dimer lattice *even* or *odd* depending on their vertex decorations. As shown in Figure 3.6, we call two dimers lying on the edges of an even (resp. odd) square an even (resp. odd) *box*; an even (resp. odd) box with two horizontal (resp. vertial) dimers corresponds to a fully uncovered black (resp. white) atom in the crystal.

One can assign weights to each edge in the dimer lattice so that the total weight of a dimer partition π, defined as[4]

$$w(\pi) = \frac{\text{product of weights of dimerized edges in } \pi}{\text{product of weights of dimerized edges in the ground state of the lattice}}\,, \qquad (3.3.6)$$

agrees with the pyramid partition weight $q_w^{w_w(\pi)} q_b^{w_b(\pi)}$. To implement such a weighting, it is sufficient to ensure that the ratio of horizontal to vertical edges in every odd and even square, respectively, equals q_w and q_b^{-1} — corresponding to white atoms being removed and black atoms being replaced.

Here, it is most convenient to use a weighting that is n-dependent. Vertical edges are always assigned weight 1. For the horizontal edges, we draw two diagonals on the dimer lattice, which pass through the lowermost and uppermost odd blocks in the ground

[4]Technically, both the numerator and denominator in this definition must be "regularized." For a given state π, one fixes a large box in the dimer lattice so that all dimers outside the box match the ground state (corresponding to an unmelted pyramid of length n); then one only multiplies together the weights of dimers inside this box.

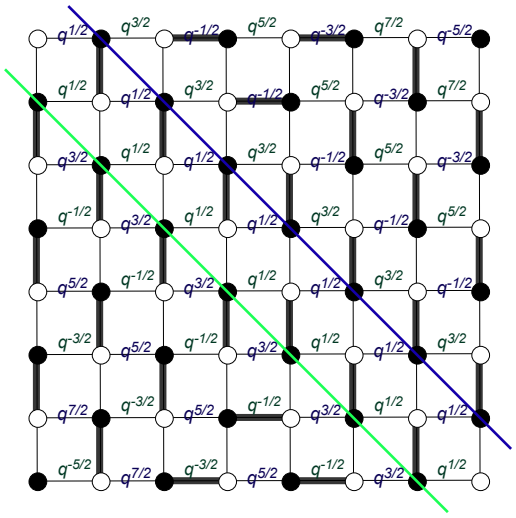

Figure 3.7: The weights assigned to edges of the dimer lattice of "length n," for $n = 2$. (The $n = 2$ ground state has been shaded in.) All vertical edges have weight 1 and all horizontal edges have an additional factor of $(-Q)^{-1/2}$.

state dimer (*i.e.* the lowermost and uppermost uncovered white atoms in the unmelted pyramid). For positive integers a, the horizontal edges $2a-1$ units above and $2a$ units below the lower diagonal are assigned weights $q^{(2a-1)/2}(-Q)^{-1/2}$ and $q^{-(2a-1)/2}(-Q)^{-1/2}$, respectively, where $a = 0$ means that an edge is touching the diagonal. Likewise the horizontal edges $2a-1$ units below and $2a$ units above the upper diagonal are assigned weights $q^{(2a-1)/2}(-Q)^{-1/2}$ and $q^{-(2a-1)/2}(-Q)^{-1/2}$, respectively. An example is shown in Figure 3.7. For a dimer model corresponding to a length-n crystal, one can check that the ratios of horizontal to vertical edges in every odd block is indeed $-q^n Q^{-1} = q_w$, and in every even block the ratio is $-q^{n-1}Q^{-1} = q_b^{-1}$. Since the resulting weight function itself is n-dependent in terms of variables q and Q, let us call it w_n rather than w.

We let the weight w_n be a function acting linearly on formal sums of partitions, and define $\Theta^{(n)}$ to be the formal sum of all possible partitions of a dimer lattice with asymptotic boundary conditions corresponding to the length-n crystal. Then

$$Z(q_a, q_b; C_n) = \sum_{\pi} q_w^{w_w(\pi)} q_b^{w_b(\pi)} = w_n(\Theta^{(n)})\,. \tag{3.3.7}$$

The operation that we claim is the combinatorial equivalent of wall crossing is described in [76] as *dimer shuffling*. It maps partitions of length n to partitions of length $n+1$. To define it, first consider an operation $\tilde{S}$, which maps a dimer state $\tilde{\pi}^{(n)}$, all of whose odd

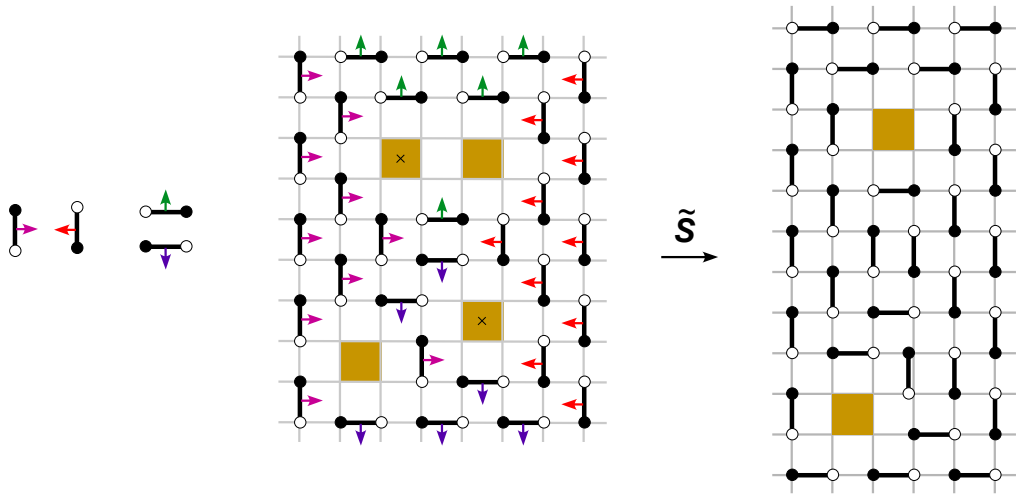

Figure 3.8: The directions in which dimers move under the shuffle $\tilde{S}$, and an example of shuffling a partition of length $n = 2$ with odd boxes deleted.

blocks have been deleted, to a dimer state $\tilde{\pi}^{(n+1)}$, all of whose even blocks are deleted. By "deleted" we mean that any dimers forming odd (resp. even) blocks are removed. The operation $\tilde{S}$ simply moves every non-deleted dimer one unit to the left, right, up, or down, according to the rules on the left side of Figure 3.8. We show an example of such a shuffling in Figure 3.8 as well; note that dimers carry their vertex decorations with them when they move. As a function from the set of {dimer partitions with odd blocks deleted} to the set of {dimer partitions with even blocks deleted}, $\tilde{S}$ is bijective [76, 81]. The actual dimer shuffling operation S can then be defined to act on finite "subsums" in $\Theta^{(n)}$. It maps each formal sum[5] of 2^m dimer states with a fixed set of m odd blocks (for any m) to the finite formal sum of all dimer states with a fixed set of even blocks in the obvious way: by deleting odd blocks, applying $\tilde{S}$, and filling in the missing even blocks in all possible combinations. Letting S act linearly on all such formal sub-sums of $\Theta^{(n)}$, it must, because $\tilde{S}$ is bijective, send $\Theta^{(n)}$ precisely to $\Theta^{(n+1)}$.

What happens to weights under dimer shuffling? We defined our weight function above so that the dimers in a partition $\tilde{\pi}$ of a length-n model with odd boxes deleted do not change weight at all under the action of $\tilde{S}$. In other words, $w_n(\tilde{\pi}) = w_{n+1}(\tilde{S}(\tilde{\pi}))$. The only change in weights of a genuine dimer state π under the action of S arises from the deletion of odd blocks and the subsequent creation of new even blocks after shuffling. An important

[5]We could also define shuffling, as in [76], to act on individual π's, but this is unnecessary.

lemma in [76] (which we will refine later in this section) is that the difference between the number of deleted odd blocks in $\tilde{\pi}$ and the missing even blocks in $\tilde{S}(\tilde{\pi})$ is always exactly n. Then a quick exercise shows that for a fixed $\tilde{\pi}$ with m deleted odd blocks,

$$w_n(\text{sum of } \pi \text{ s.t. } \pi \text{ agrees with } \tilde{\pi}) = (1 - q^n Q^{-1})^m \cdot w_n(\tilde{\pi})\,, \tag{3.3.8}$$

$$w_{n+1}(\text{sum of } \pi \text{ s.t. } \pi \text{ agrees with } \tilde{S}(\tilde{\pi})) = (1 - q^n Q^{-1})^{m-n} \cdot w_{n+1}(\tilde{S}(\tilde{\pi}))\,. \tag{3.3.9}$$

(By "agrees with," we mean aside from deleted blocks.) The ratio of these quantities is independent of m, immediately proving that

$$w_n(\Theta^{(n)}) = (1 - q^n Q^{-1})^n w_{n+1}(\Theta^{(n+1)})\,. \tag{3.3.10}$$

This is precisely the wall-crossing formula between chambers C_n for the conifold.

Formula (3.3.10) suggests (correctly) that we can write the crystal or dimer partition function for a model of length n as

$$w_n(\Theta^{(n)}) = \prod_{j=n}^{\infty} (1 - q^j Q^{-1})^j \cdot w_\infty(\Theta^{(\infty)})\,. \tag{3.3.11}$$

Of course, the quantity $w_\infty(\Theta^{(\infty)})$ must be the Donaldson-Thomas partition function of the conifold, and this relation holds because pyramid partitions of length $n \to \infty$ effectively reduce to the topological vertex formalism of [24, 25] (see also [74, 9, 10]).

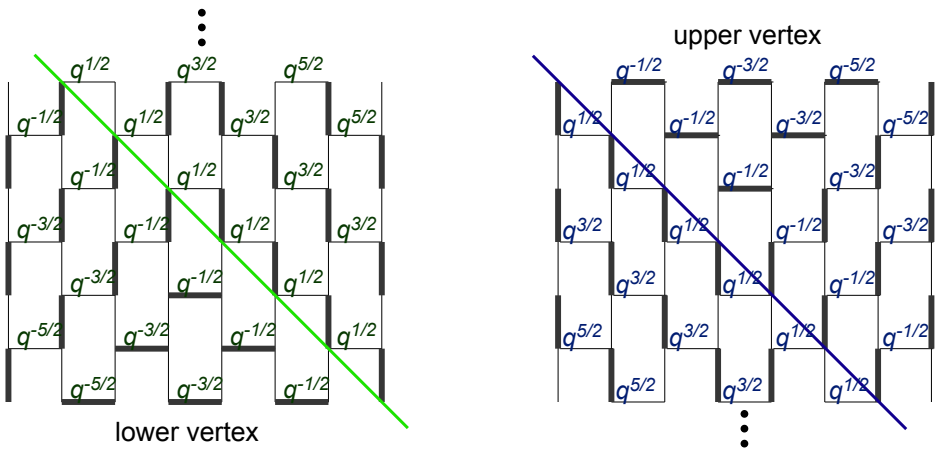

Figure 3.9: The brick-like lattices around the upper and lower vertices as $n \to \infty$. The ground state state of the dimer is shaded in. As before, each horizontal edge also carries a weight of $(-Q)^{-1/2}$

To understand this relation, consider the n-dependent weighting system of Figure 3.7. In the limit $n \to \infty$, the weights of half the edges around the lower vertex (of the pyramid,

or of the dimer model) acquire infinitely large, positive powers of q and cease to contribute to the partition function. Likewise for half the edges around the upper vertex. Therefore, the only dimer partitions around these vertices that can contribute to the length-infinity partition function involve dimers on edges of the brick-like lattices of Figure 3.9. These brick-like lattices, however, are equivalent to hexagonal dimer lattices, which correspond to the three-dimensional cubic partitions that arise in the topological vertex.

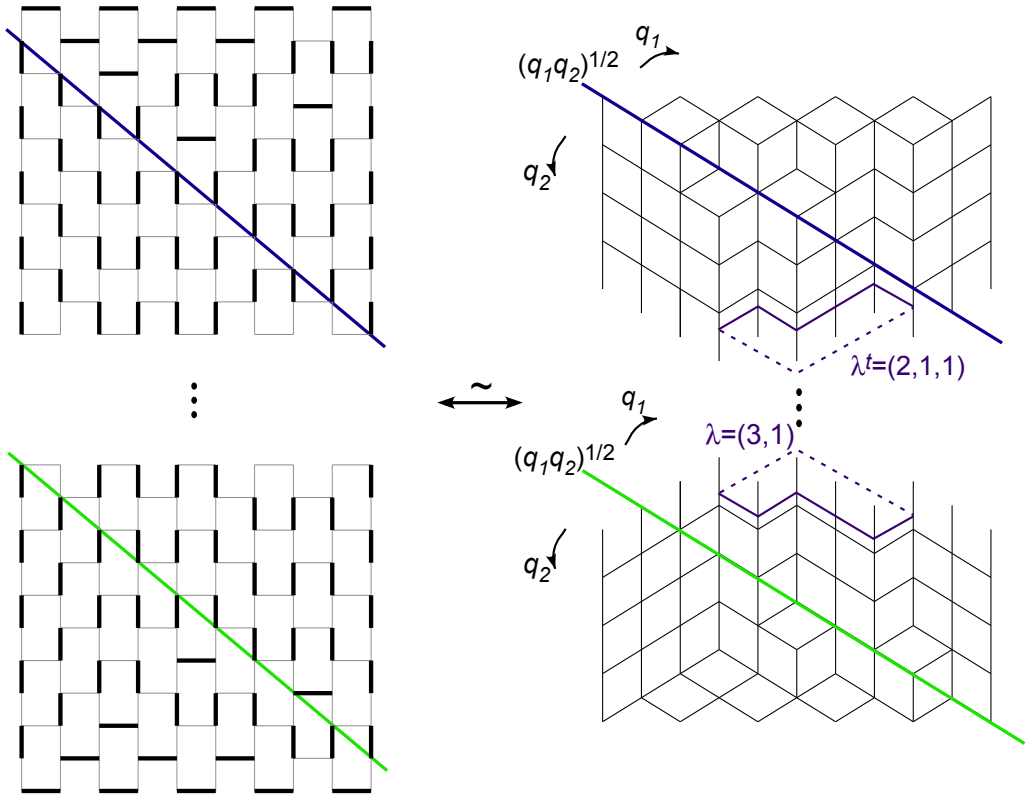

Figure 3.10: The map between the length-infinity dimer model and a pair of topological vertices. (The extra q_1 and q_2 notations are for the refined case in Section 3.4.)

As argued more carefully in [76], any (nontrivial) configuration of the length-infinity dimer model can be constructed via a series of moves that amount to 1) cutting out a Young diagram λ simultaneously from the upper and lower vertices, 2) stacking up individual boxes to form a cubic partition π_λ^- around the lower vertex, and 3) stacking up boxes to form a partition π_λ^+ around the upper vertex. An example of such a dimer configuration and its corresponding topological vertex partitions is shown in Figure 3.10. By observing how dimers shift in these three steps and using our $n \to \infty$ weighting, it is not too hard to

see that the contributions to the partition function are $(-Q)^{|\lambda|}q^{\frac{1}{2}||\lambda||^2}q^{\frac{1}{2}||\lambda^t||^2}$ from step (1), $q^{|\pi^-_\lambda|}$ from step (2), and $q^{|\pi^+_{\lambda^t}|}$ from step (3).[6] Therefore, the total partition function is

$$w_\infty(\Theta^{(\infty)}) = \sum_\lambda \sum_{\pi^+_{\lambda^t},\,\pi^-_\lambda} (-Q)^{|\lambda|} q^{\frac{1}{2}||\lambda||^2+\frac{1}{2}||\lambda^t||^2} q^{|\pi^+_{\lambda^t}|+|\pi^-_\lambda|}\,, \tag{3.3.12}$$

which is *precisely* the topological vertex expression for the (unreduced) partition function of the conifold [24, 25]. In terms of Schur functions, the generating function for three-dimensional cubic partitions with a single nontrivial asymptotic boundary condition λ is $\sum_{\pi_\lambda} q^{|\pi_\lambda|} = M(q)\, q^{-\frac{1}{2}||\lambda||^2} s_{\lambda^t}(q^{-\rho}) = M(q)\, q^{-\frac{1}{2}||\lambda||^2} s_{\lambda^t}(q^{1/2}, q^{3/2}, q^{5/2}, ...)$. Thus, as expected,

$$\begin{aligned} w_\infty(\Theta^{(\infty)}) &= Z(q, Q; C_\infty) \\ &= M(q)^2 \sum_\lambda (-Q)^\lambda s_\lambda(q^{-\rho}) s_{\lambda^t}(q^{-\rho}) \qquad (3.3.13) \\ &= M(q)^2 \prod_{j,k=1}^{\infty} (1 - q^{j-1/2} q^{k-1/2} Q) \qquad (3.3.14) \\ &= M(q)^2 \prod_{j=1}^{\infty} (1 - q^j Q)^j\,. \end{aligned}$$

3.4 Refined crystals

We finally come to the crystal-melting models for refined invariants. We will first describe the models that compute the refined partition functions in all chambers C_n and $\tilde{C}_n$ for the conifold. Then, generalizing Section 3.3, we will prove the formulas in chambers C_n by showing that a refined version of dimer shuffling leads to refined wall crossing. We also show that as $n \to \infty$ refined pyramid partitions reduce to a pair of refined topological vertices.

At the level of crystal models, one must draw a series of diagonals on the pyramid partition, and interpolate weights between the variable q_1 on one side of the diagonals and q_2 on the other. To be more specific, consider the pyramid of length $n = 1$, corresponding to the Szendröi chamber C_1. On this crystal model, we draw a single diagonal as shown in

[6] We use conventional notation for Young diagrams and three-dimensional cubic partitions; λ^t is the transpose of the diagram λ, the rows of λ have lengths λ_i, $|\lambda| = \sum \lambda_i$ is the number of boxes in λ, $||\lambda||^2 = \sum \lambda_i^2$, and $|\pi|$ is the number of boxes in a three-dimensional partition.

Figure 3.11; we assign white atoms above the diagonal a weight q_w^+, white atoms below the diagonal a weight q_w^-, and white atoms on the diagonal itself a weight $(q_w^+ q_w^-)^{1/2}$. All black atoms are assigned weight q_b. Letting $w_w^+(\pi)$, $w_w^-(\pi)$, and $w_w^0(\pi)$ be the numbers of white atoms above, below, and on the diagonal, respectively, in the partition π, and identifying $q_w^+ = -q_1 Q^{-1}$, $q_w^- = -q_2 Q^{-1}$, and $q_b = -Q$, we find

$$\begin{aligned} Z(q_w^+, q_w^-, q^b; C_1) &= \sum_\pi (q_w^+)^{w_w^+(\pi)} (q_w^-)^{w_w^-(\pi)} (q_w^+ q_w^-)^{\frac{1}{2} w_w^0(\pi)} q_b^{w_b(\pi)} \\ &= Z^{ref}(q_1, q_2, Q; C_1) \\ &= M(q_1, q_2)^2 \prod_{i,j=1}^{\infty} (1 - q_1^{i-\frac{1}{2}} q_2^{j-\frac{1}{2}} Q)(1 - q_1^{i-\frac{1}{2}} q_2^{j-\frac{1}{2}} Q^{-1}) \,. \end{aligned} \tag{3.4.1}$$

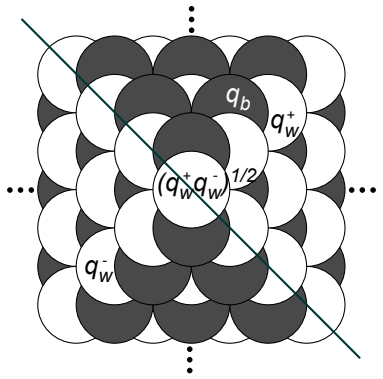

Figure 3.11: Weights of atoms for the refined partition function in chamber C_1.

To generalize to the length-n pyramid, we draw n diagonals, as in the left half of Figure 3.12. It is more natural to work directly in terms of the variables q_1, q_2, and Q. We assign weights $-q_1^n Q^{-1}$ (resp. $-q_1^{-(n-1)} Q$) to the white (resp. black) atoms above all the diagonals and weights $-q_2^n Q^{-1}$ (resp. $-q_2^{-(n-1)} Q$) to the white (resp. black) atoms below all the diagonals. The diagonals themselves intersect white atoms; we assign the same weight to all the white atoms on a single diagonal, interpolating between $-q_1^{n-\frac{1}{2}} q_2^{\frac{1}{2}} Q^{-1}$ on the uppermost diagonal and $-q_1^{\frac{1}{2}} q_2^{n-\frac{1}{2}} Q^{-1}$ on the lowermost (multiplying by $q_1^1 q_2^{-1}$ in each intermediate step). Similarly, black atoms lie between diagonals, and we assign them weights ranging from $-q_1^{-n+\frac{3}{2}} q_2^{-\frac{1}{2}} Q$ directly below the upper diagonal to $-q_1^{-\frac{1}{2}} q_2^{-n+\frac{3}{2}} Q$ directly above the lower diagonal. Multiplying together the weights of all atoms removed in

a given partition π and summing these quantities over partitions, we obtain the expected

$$Z^{ref}(q_1, q_2, Q; C_n) = M(q_1, q_2)^2 \prod_{i,j=1}^{\infty} (1 - q_1^{i-\frac{1}{2}} q_2^{j-\frac{1}{2}} Q) \prod_{\substack{i\geq 1,\, j\geq 1 \\ i+j>n}} (1 - q_1^{i-\frac{1}{2}} q_2^{j-\frac{1}{2}} Q^{-1}) \,. \quad (3.4.2)$$

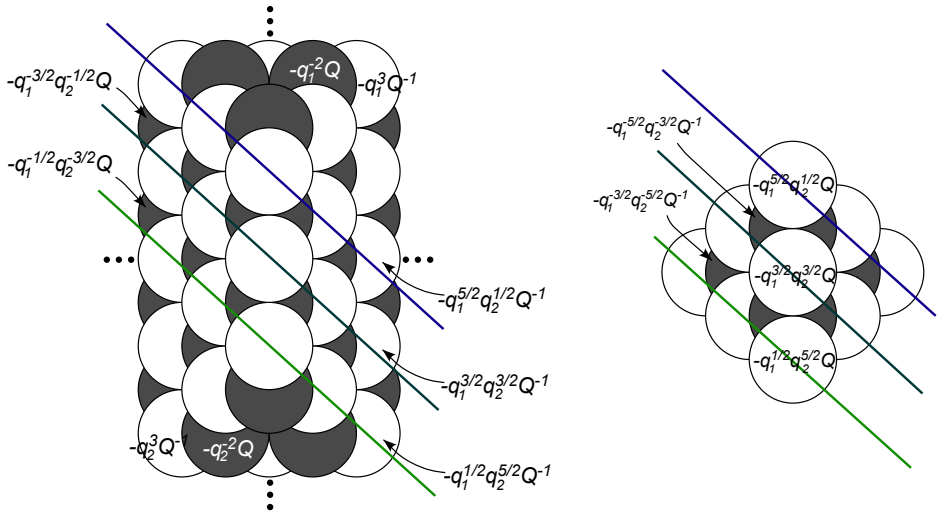

Figure 3.12: Refined weights of atoms for chambers C_n and $\tilde{C}_n$, with $n = 3$.

For chambers $\tilde{C}_n$, the finite pyramid of length n can also be split by n diagonals, as shown in the right half of Figure 3.12. If one assigns weights such that (1) when $q_1 \to q$ and $q_2 \to q$ white atoms have weight $-q^n Q$ and black atoms have weight $-q^{-(n+1)}Q^{-1}$; (2) when moving up one step, either on or inbetween diagonals, the absolute value of the power of q_2 (resp. q_1) decreases (resp. increases) by 1; and (3) the assignment is symmetric about the middle diagonal(s) of the crystal, the resulting partition function is precisely

$$Z^{ref}(q_1, q_2, Q; \tilde{C}_n) = M(q_1, q_2)^2 \prod_{\substack{i\geq 1,\, j\geq 1 \\ i+j\leq n+1}} (1 - q_1^{i-\frac{1}{2}} q_2^{j-\frac{1}{2}} Q) \,.$$

For the remainder of the section we return to the infinite pyramid of length n, generalizing the previous unrefined discussion to refine the connection between shuffling, wall crossing, and the refined topological vertex (and to prove formula (3.4.2)). We first observe that in order to equate refined pyramid partitions and their weights with states (configurations) of a dimer lattice, we can use almost the same n-dependent weighting described in Figure 3.7. Now, for positive integers a, the horizontal edges $2a-1$ units above and $2a$ units below the lower diagonal are assigned weights $q_1^{(2a-1)/2}(-Q)^{-1/2}$ and $q_2^{-(2a-1)/2}(-Q)^{-1/2}$,

respectively. Likewise the horizontal edges $2a-1$ units below and $2a$ units above the upper diagonal are assigned weights $q_2^{(2a-1)/2}(-Q)^{-1/2}$ and $q_1^{-(2a-1)/2}(-Q)^{-1/2}$. See the example in Figure 3.13.

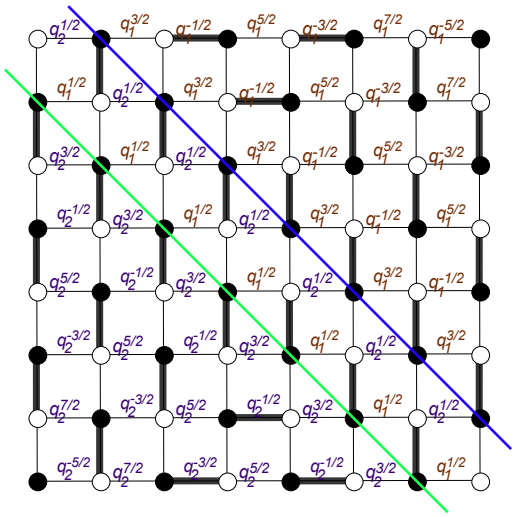

Figure 3.13: Refined weighting of the length-n dimer, for $n = 2$.

As in the unrefined case, the weights of dimers which are not part of deleted odd or even blocks do not change during dimer shuffling $\tilde{S}$, due to our n-dependent weighting. In order to understand the behavior of the deleted blocks, we observe that the shuffling $\tilde{S}$ removes *exactly* one (deleted) odd block from each of the n diagonals of a dimer configuration of length n. Moreover, the remaining (deleted) odd blocks are mapped to deleted even blocks with exactly the same weights — if (for instance) they were above all the diagonals, then they remain above all the diagonals. These statements can be proved with careful counting arguments, considering the number of dimers on and around each diagonal in an arbitrary configuration before and after shuffling. The result is that when the actual shuffling S maps a formal sum of states π agreeing with a fixed odd-deleted state $\tilde{\pi}$ on all but their odd blocks to a formal sum of states agreeing on all but their even blocks, the weight of this formal sum changes by exactly $\prod_{i+j=n+1}(1 - q_1^{i-\frac{1}{2}} q_2^{j-\frac{1}{2}} Q^{-1})$; therefore,

$$w_n(\Theta^{(n)}) = \prod_{\substack{i\geq 1,\, j\geq 1 \\ i+j=n+1}} (1 - q_1^{i-\frac{1}{2}} q_2^{j-\frac{1}{2}} Q^{-1}) \cdot w_{n+1}(\Theta^{(n+1)}) \,. \tag{3.4.3}$$

This, of course, is the refined wall-crossing formula for chambers C_n.

The crystal-melting or dimer partition function of length n can now be written as

$$w_n(\Theta^{(n)}) = \prod_{i,j=1}^{\infty} (1 - q_1^{i-\frac{1}{2}} q_2^{j-\frac{1}{2}} Q^{-1}) \cdot w_\infty(\Theta^{(\infty)}) \,. \tag{3.4.4}$$

The last term, $w_\infty(\Theta^{(\infty)})$, is obtained from a slightly modified version of the refined topological vertex of [26]. To see this, observe that as $n \to \infty$ the neighborhoods of the upper and lower vertices of the dimer lattice still reduce to effective brick-like lattices, now shown in Figure 3.14. In terms of three-dimensional cubic partitions, states of the length-infinity dimer are again created by 1) cutting out a Young diagram λ simultaneously from the upper and lower vertices, 2) stacking up individual boxes to form a cubic partition π_λ^- around the lower vertex, and 3) stacking up boxes to form a partition π_λ^+ around the upper vertex. The creation of the Young diagram λ comes with a fairly simple weight $(-Q)^{|\lambda|} q_1^{\frac{1}{2}||\lambda||^2} q_2^{\frac{1}{2}||\lambda^t||^2}$. However, both the upper and lower "room corners" are now split along a diagonal, as shown in Figure 3.10. In the case of the lower corner, boxes stacked below the diagonal come with

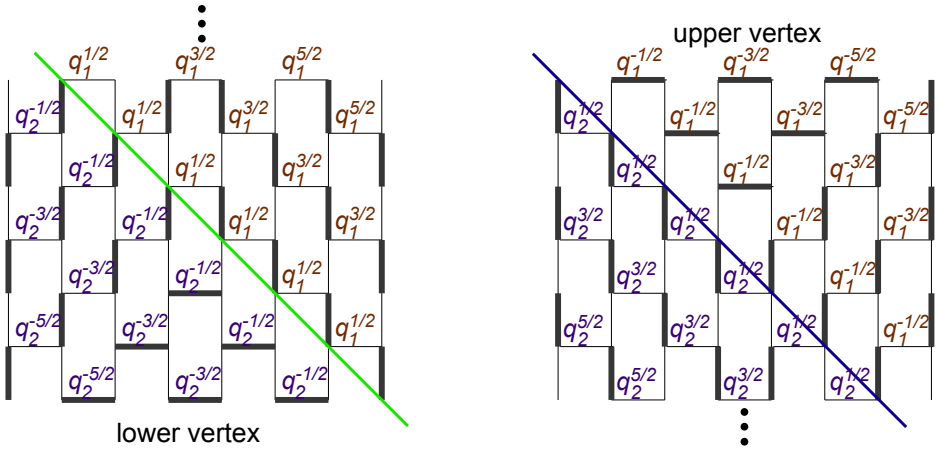

Figure 3.14: Neighborhoods of the refined upper and lower vertices as $n \to \infty$.

weight q_2, those above the diagonal with weight q_1, and those that the diagonal intersects have weight $(q_1 q_2)^{\frac{1}{2}}$. The situation is reversed for the upper vertex. The generating function for such three-dimensional cubic partitions with one asymptotic boundary condition λ is (for example, at the lower vertex)

$$\sum_{\pi_\lambda} q_1^{|\pi_\lambda|^{(q_1)}} q_2^{|\pi_\lambda|^{(q_2)}} (q_1 q_2)^{\frac{1}{2}|\pi_\lambda|^{(0)}} = M(q_1, q_2)\, q_2^{-\frac{1}{2}||\lambda^t||^2} s_\lambda(q_2^{-\rho}) \,, \tag{3.4.5}$$

with $M(q_1, q_2) = \prod_{i,j=1}^{\infty} (1 - q_1^{i-\frac{1}{2}} q_2^{j-\frac{1}{2}})^{-1}$. Therefore, the length-infinity pyramid partition

function is

$$
\begin{aligned}
w_\infty(\Theta^{(\infty)}) &= \sum_\lambda \sum_{\pi^+_{\lambda^t},\pi^-_\lambda} (-Q)^{|\lambda|}\, q_1^{\frac{1}{2}||\lambda||^2} q_2^{\frac{1}{2}||\lambda^t||^2} \\
&\qquad \times q_1^{|\pi^-_\lambda|^{(q_1)}} q_2^{|\pi^-_\lambda|^{(q_2)}} (q_1q_2)^{\frac{1}{2}|\pi^-_\lambda|^{(0)}}\, q_2^{|\pi^+_{\lambda^t}|^{(q_2)}} q_1^{|\pi^+_{\lambda^t}|^{(q_1)}} (q_1q_2)^{\frac{1}{2}|\pi^+_{\lambda^t}|^{(0)}} \\
&= M(q_1,q_2)^2 \sum_\lambda (-Q)^{|\lambda|} s_\lambda(q_2^{-\rho}) s_{\lambda^t}(q_1^{-\rho}) \\
&= M(q_1,q_2)^2 \prod_{i,j=1}^\infty (1 - q_1^{i-\frac{1}{2}} q_2^{j-\frac{1}{2}} Q)\,. \qquad (3.4.6)
\end{aligned}
$$

Note that expression (3.4.5) differs very slightly from the refined topological vertex used in [26] (with the boundary condition λ placed along an "unpreferred" direction). The difference comes from our symmetric choice of normalization, as discussed in Section 3.1. In [26] the diagonal is assigned to q_2 rather than $(q_1q_2)^{\frac{1}{2}}$, resulting in the fact that the refined MacMahon function appearing in the analogue of (3.4.5) is not $M(q_1,q_2) = \prod_{i,j=1}^\infty (1 - q_1^{i-\frac{1}{2}} q_2^{j-\frac{1}{2}})^{-1}$, but rather $M_{-1}(q_1,q_2) = \prod i,j = 1^\infty (1 - q_1^{i-1} q_2^j)^{-1}$ (*cf.* (3.1.23)). The refined A-model (Gromov-Witten/Gopakumar-Vafa) partition functions calculated with the refined vertex are always normalized by the prefactor $M(q_1,q_2)^{\chi}(X)$, so in many previous calculations this has made no difference.

Chapter 4

Refined = Motivic

Despite its obvious conceptual advantages, the direct interpretation of $\mathcal{H}_{BPS}$ as the cohomology of a moduli space of D-branes or representations of a quiver discussed in Section 2.3 does *not* generally work. Thinking in terms of quiver representations, and even putting aside the issue of noncompact moduli spaces (working, for example, with nice rigid noncompact toric Calabi-Yau's), the general problem is that the moduli spaces $\mathcal{M}(\gamma)$ are highly singular. In particular, $\mathcal{M}(\gamma)$ is defined as the quotient of an algebraic variety by a "gauge group" $\prod_i GL(n_i)$, so it is mathematically a moduli stack (*not* a variety). It is often not clear how to compute its cohomology, or even its Euler characteristic.

Kontsevich and Soibelman address this problem in both unrefined and (we argue) refined cases in [15]. They work with quiver descriptions of Calabi-Yau's and D-branes, using a stability condition very similar to II-stability[1] to define generalized Donaldson-Thomas invariants. These invariants should reproduce physical BPS indices $\Omega(\gamma; t_\infty)$ in all chambers of Kähler moduli space $\mathcal{M}_V$, in a type IIA duality frame. In [34], it was proven that this is indeed the case in a rigid limit of 4-dimensional supergravity.

Kontsevich and Soibelman also define a "q-deformed" version of the generalized Donaldson-Thomas invariants: the motivic Donaldson-Thomas invariants. They essentially use motivic integration as a well-defined alternative to calculating the cohomology of moduli spaces. Note, however, that motivic integration can be thought of (from one point of view) as cutting up a space into copies of the noncompact affine line $\mathbb{L}$, the affine plane $\mathbb{L}^2$, the

[1] *I.e.* a stability condition based on comparing arguments of central charges of states, also similar to Denef stability (2.2.1).

affine space $\mathbb{L}^3$, etc. The motivic DT invariants are functions of $\mathbb{L}^{1/2}$, the square root of the motive of the affine line. One can also use the Schur functor to pass from motivic to "quantum" invariants, replacing $\mathbb{L}^{1/2}$ with the quantum variable $-q^{1/2}$. As $q^{1/2} \to -1$, the motivic invariants reduce to the classical generalized Donaldson-Thomas invariants. Our main conjecture is that motivic DT invariants are equivalent to refined invariants in any chamber of moduli space, with

$$\boxed{\mathbb{L}^{1/2} \quad \longleftrightarrow \quad -q^{1/2} \quad \longleftrightarrow \quad y}\,. \tag{4.0.1}$$

Why should this be true? Besides the potentially naive fact that both motivic and refined invariants are fairly natural deformations of the classical BPS indices/invariants, we will argue in this chapter that motivic and refined invariants have identical wall crossing behavior. In Section 4.1, we will review the classical and motivic wall-crossing formulas from [15], and then show in Section 4.2 that motivic wall crossing implies primitive and semi-primitive refined wall crossing. In Section 4.3, we will provide several very explicit examples of the equivalence between refined and motivic invariants in the context of $SU(2)$ Seiberg-Witten theory with $N_f = 0, 1, 2, 3$ flavors — using geometric engineering [82] to view Seiberg-Witten theory as a rigid limit of string theory compactified on a local Calabi-Yau. The results of this chapter are based on work in [1, 2].

There also exists direct evidence for the equivalence of refined and motivic invariants coming from knot theory and the interpretation of knot homologies via BPS invariants of Calabi-Yau threefolds, as in [29, 30]. In [83], motivic invariants were related to knot Floer homology. We hope to investigate the motivic nature of knot homologies further in the future.

4.1 Classical and motivic KS wall crossing

We begin by reviewing the classical (or unrefined) and motivic wall-crossing formulas of Kontsevich and Soibelman [15]. In the classical case, we borrow some of the notation and formalism of [34].

Classical

The classical wall-crossing formula generalizes both the primitive (2.2.6) and semiprimitive (2.2.12) cases derived physically in Section 2.2. It encodes the degeneracies of BPS states in a given chamber of moduli space $\mathcal{M}_V$ in terms of a non-commuting product of symplectomorphisms acting on a complexified charge lattice.

Specifically, let Γ be the lattice of D-brane charges (as above), let $\Gamma^\vee$ be its dual, and let

$$\mathbf{T}_\Gamma = \Gamma^\vee \otimes \mathbb{C}^* \tag{4.1.1}$$

be an r-dimensional complex torus, where r is the rank of Γ. One can define functions X_γ on this complex torus corresponding to any $\gamma \in \Gamma$, acting as $X_\gamma : \sum C_a \gamma_a^\vee \mapsto \exp \sum C_a \gamma_a^\vee(\gamma)$. These satisfy $X_\gamma X_{\gamma'} = X_{\gamma+\gamma'}$, and if $\{\gamma_i\}$ is any basis of Γ, the corresponding $X_i = X_{\gamma_i}$ will be coordinates on $\mathbf{T}_\Gamma$. The complex torus can moreover be endowed with a natural symplectic structure

$$\omega = \frac{1}{2}\langle \gamma_i, \gamma_j \rangle^{-1} \frac{dX_i}{X_i} \wedge \frac{dX_j}{X_j}\,, \tag{4.1.2}$$

where $\langle \gamma_i, \gamma_j \rangle^{-1}$ is the inverse of the intersection form on Γ (in any chosen basis).

Under this symplectic structure, the family of maps $\{U_\gamma\}_{\gamma\in\Gamma}$,

$$\begin{aligned} \mathbf{T}_\Gamma &\to \mathbf{T}_\Gamma \\ U_\gamma : X_{\gamma'} &\mapsto X_{\gamma'}(1-\sigma(\gamma)X_\gamma)^{\langle \gamma', \gamma\rangle}\,. \end{aligned} \tag{4.1.3}$$

are classical symplectomorphisms. The coefficient $\sigma(\gamma)$ is just a sign ± 1; choosing an electric-magnetic duality frame (or symplectic splitting)[2] for Γ and writing $\gamma = \gamma_e + \gamma_m$, this coefficient equals $(-1)^{\langle \gamma_e, \gamma_m\rangle}$. If one defines vector fields e_γ to be the infinitesimal symplectomorphisms generated by the Hamiltonians $\sigma(\gamma)X_\gamma$, then the e_γ's generate a Lie algebra with relations

$$[e_{\gamma_1}, e_{\gamma_2}] = (-1)^{\langle \gamma_1, \gamma_2\rangle}\langle \gamma_1, \gamma_2\rangle e_{\gamma_1+\gamma_2}\,, \tag{4.1.4}$$

and the symplectomorphism U_γ can be expressed as

$$U_\gamma = \exp \mathrm{Li}_2(e_\gamma)\,. \tag{4.1.5}$$

[2]Technically, one needs to take the charge lattice Γ and the corresponding torus $\mathbf{T}_\Gamma$ to be fibered over the moduli space $\mathcal{M}_V$, and an electric-magnetic split only works locally. However, this issue is relatively unimportant for the present discussion — it would only be relevant if one were interested in crossing walls all the way around a singularity in $\mathcal{M}_V$. See [15] and [34] for further discussion.

Here, $\mathrm{Li}_2(x) = \sum_{n=1}^{\infty} \frac{x^n}{n^2}$ is the classical Euler dilogarithm function.

Now, for a given Calabi-Yau, a point t (*i.e.* t_∞) in Kähler moduli space $\mathcal{M}_V$, and a ray in the charge lattice generated by a primitive charge γ, one forms the composite symplectomorphism

$$A_\gamma(t) = \prod_{\gamma' \in \mathrm{ray}} U_{\gamma'}^{\Omega(\gamma';t)} = \prod_{k \geq 1} U_{k\gamma}^{\Omega(k\gamma;t)} \,. \tag{4.1.6}$$

The BPS indices $\Omega(\gamma;t)$ are exactly as in (2.1.27), and this product is over all stable BPS states in the ray (otherwise $\Omega(\gamma;t)$ obviously vanishes). Notice that $U_{d\gamma}$ and $U_{d'\gamma}$ commute for any d, d'. The statement of wall crossing is that the product over all rays of states whose central charges become aligned at a wall of marginal stability,

$$A(t) = \overset{\curvearrowright}{\prod_{\mathrm{rays}\,\gamma}} A_\gamma(t) = \overset{\curvearrowright}{\prod_{\mathrm{states}\,\gamma'}} U_{\gamma'}^{\Omega(\gamma';t)} \,, \tag{4.1.7}$$

taken in order of *increasing phase of the central charge* $Z(\gamma,t)$, is the same on both sides of the wall.[3] In other words, going from $t = t_+$ on one side of the wall to $t = t_-$ on the other, both the BPS indices and the ordering will change but the overall product will remain the same:

$$\boxed{\overset{\curvearrowright}{\prod_{\gamma}} U_{\gamma'}^{\Omega(\gamma',t_+)} = \overset{\curvearrowright}{\prod_{\gamma'}} U_{\gamma'}^{\Omega(\gamma,t_-)}} \,. \tag{4.1.8}$$

Motivic

To simplify the description of motivic invariants, we use the Serre functor to pass from the motive $\mathbb{L}^{1/2}$ to the quantum variable $-q^{1/2}$, as explained in [15]. The motivic DT invariants can then be defined as automorphisms of a quantum torus.

The quantum torus $\widehat{\mathbf{T}}_\Gamma$ in question is simply the quantization of (4.1.1), using the symplectic structure (4.1.2). The Lie algebra (4.1.4) is q-deformed to an associative algebra generated by operators $\{\hat{e}_\gamma\}_{\gamma \in \Gamma}$, such that

$$\hat{e}_{\gamma_1} \hat{e}_{\gamma_2} = q^{\frac{1}{2}\langle \gamma_1, \gamma_2 \rangle} \; \hat{e}_{\gamma_1 + \gamma_2} \tag{4.1.9}$$

and $\hat{e}_0 = 1$. In particular, these generators obey the commutation relations

$$[\hat{e}_{\gamma_1}, \hat{e}_{\gamma_2}] = \left(q^{\frac{1}{2}\langle \gamma_1, \gamma_2 \rangle} - q^{-\frac{1}{2}\langle \gamma_1, \gamma_2 \rangle} \right) \hat{e}_{\gamma_1 + \gamma_2} \,. \tag{4.1.10}$$

[3] Being more careful, one must make a choice of "particles" vs. "antiparticles" and only include the former in this product; so exactly half the rays that align really contribute. This will become clear in the examples of Sections 4.2 and 4.3.

In the "classical limit" $q^{1/2} \to -1$, one finds that

$$\lim_{q^{1/2}\to -1} (q-1)^{-1} \left(q^{\frac{1}{2}\langle \gamma_1,\gamma_2\rangle} - q^{-\frac{1}{2}\langle \gamma_1,\gamma_2\rangle} \right) = (-1)^{\langle \gamma_1,\gamma_2\rangle} \langle \gamma_1,\gamma_2\rangle \,, \tag{4.1.11}$$

so that the elements

$$e_\gamma := \lim_{q^{1/2}\to -1} \frac{\hat{e}_\gamma}{q-1} \,. \tag{4.1.12}$$

satisfy (4.1.4).

In the original work of Kontsevich and Soibelman, the motivic DT invariants were composite operators $\mathbf{A}_\gamma(t)$ associated to entire rays. These operators had Taylor expansions

$$\mathbf{A}_\gamma(t) = 1 + \frac{\Omega^{mot}(\gamma;t;q)}{q^{1/2}-q^{-1/2}}\, \hat{e}_\gamma + (\ )\, \hat{e}_\gamma^2 + \dots, \tag{4.1.13}$$

with coefficients given by motivic integrals. It has since become clear, however, that these operators have a factorization property just as in the classical case, *cf.* [84, 2]. We shall see that physically, this factorization is both necessary and natural. As in [15], let us introduce the quantum dilogarithm function

$$\mathbf{E}(x) = \sum_{n=0}^{\infty} \frac{\left(-q^{\frac{1}{2}}x\right)^n}{(1-q)\dots(1-q^n)} \,, \tag{4.1.14}$$

and define operators

$$\mathbf{U}_\gamma(\hat{e}_\gamma) = \mathbf{E}(\hat{e}_\gamma) \,. \tag{4.1.15}$$

Then, for a ray of BPS states in Γ generated by a charge γ, we have

$$\mathbf{A}_\gamma(t) = \prod_{\gamma' \in \text{ray}} \prod_{n\in\mathbb{Z}} \mathbf{U}_{\gamma'}\big((-q^{1/2})^n \hat{e}_{\gamma'}\big)^{(-1)^n \Omega_n^{mot}(\gamma';t)} \,. \tag{4.1.16}$$

$$= \prod_{k\geq 1} \prod_{n\in\mathbb{Z}} \mathbf{U}_{k\gamma}\big((-q^{1/2})^n \hat{e}_\gamma^{\,k}\big)^{(-1)^n \Omega_n^{mot}(k\gamma;t)} \,. \tag{4.1.17}$$

for (positive) integral motivic invariants $\Omega_n^{mot}(\gamma;t)$. Of course, we want to claim that $\Omega_n^{mot}(\gamma;t) = \Omega_n(\gamma;t)$ as defined in (2.1.31).

The statement of motivic wall crossing is that the product over all rays of states whose central charges become aligned at a wall of marginal stability,

$$\mathbf{A}(t) = \overset{\curvearrowright}{\prod_{\text{rays }\gamma}} \mathbf{A}_\gamma(t) = \overset{\curvearrowright}{\prod_{\text{states }\gamma'}} \prod_{n\in\mathbb{Z}} \mathbf{U}_{\gamma'}\big((-q^{1/2})^n \hat{e}_{\gamma'}\big)^{(-1)^n \Omega_n^{mot}(\gamma';t)} \,, \tag{4.1.18}$$

taking the product in order of increasing phase of central charges, is constant as the wall is crossed. Or, as in (4.1.8),

$$\boxed{\overset{\curvearrowright}{\prod_{\text{states }\gamma'}} \prod_{n\in\mathbb{Z}} \mathbf{U}_{\gamma'}\big((-q^{1/2})^n \hat{e}_{\gamma'}\big)^{(-1)^n \Omega_n^{mot}(\gamma';t_+)} = \overset{\curvearrowright}{\prod_{\text{states }\gamma'}} \prod_{n\in\mathbb{Z}} \mathbf{U}_{\gamma'}\big((-q^{1/2})^n \hat{e}_{\gamma'}\big)^{(-1)^n \Omega_n^{mot}(\gamma';t_-)}} \,. \tag{4.1.19}$$

Note that the operators $\mathbf{U}_\gamma$ and their products generate q-deformed symplectomorphisms on the quantum torus with coordinates $\{\hat{e}_\gamma\}$ via the *conjugation* action $\mathrm{Ad}_{\mathbf{U}_\gamma}$.

The quantum dilogarithm will be of central importance in Part II of this thesis, and we will examine many of its properties further in Section 8.3. For now, however, let us note that in the classical limit $q^{1/2} \to -1$ it has the asymptotic expansion

$$\mathbf{E}(x) = \exp\left(-\frac{1}{2\hbar}\mathrm{Li}_2(x) + \frac{x\hbar}{12(1-x)} + \dots\right) \tag{4.1.20}$$

where $q^{1/2} = -e^{\hbar}$, thereby relating (conjugation by) $\mathbf{U}_\gamma$ with the classical U_γ. Moreover, the function obeys a fundamental "pentagon" identity

$$\mathbf{E}(x_1)\mathbf{E}(x_2) = \mathbf{E}(x_2)\mathbf{E}(x_{12})\mathbf{E}(x_1) \tag{4.1.21}$$

when $x_1 x_2 = q x_2 x_1$ and $x_{12} = q^{-1/2} x_1 x_2 = q^{1/2} x_2 x_1$. This will provide the simplest example of motivic/refined wall crossing in Section 4.2. Finally, it will be useful to note that there exists an infinite product expansion

$$\mathbf{E}(x) = \prod_{r=0}^{\infty} (1 + q^{r+\frac{1}{2}} x)^{-1}\,, \tag{4.1.22}$$

equivalent to the sum (4.1.14).

4.2 Refined = Motivic

We now show that the motivic wall-crossing formula (4.1.19) is equivalent to the refined physical formulas (2.2.7)-(2.2.13) in primitive and semi-primitive cases, with $\boxed{-q^{1/2} = y}$. Since the motivic formula reduces to the classical formula (4.1.8) in the limit $q^{1/2} \to -1$, this also constitutes an alternative proof that the classical KS formula agrees with unrefined physical wall crossing. The primitive and semi-primitive arguments given here appear in our work [1, 2].

Warmup

We begin with the pentagon identity (4.1.21). This can be interpreted as crossing a wall where two primitive hypermultiplets with charges γ_1 and γ_2, satisfying

$$\langle \gamma_1, \gamma_2 \rangle = 1 \tag{4.2.1}$$

form a bound state. The corresponding local quiver for this wall is shown in Figure 4.1. Since $\hat{e}_{\gamma_1}\hat{e}_{\gamma_2} = q\,\hat{e}_{\gamma_1}\hat{e}_{\gamma_2}$, the pentagon identity implies a wall-crossing formula

$$\mathbf{U}_{\gamma_1}(\hat{e}_{\gamma_1})\,\mathbf{U}_{\gamma_2}(\hat{e}_{\gamma_2}) = \mathbf{U}_{\gamma_2}(\hat{e}_{\gamma_2})\,\mathbf{U}_{\gamma_1+\gamma_2}(\hat{e}_{\gamma_1+\gamma_2})\,\mathbf{U}_{\gamma_1}(\hat{e}_{\gamma_1})\,. \tag{4.2.2}$$

Since these two products are taken in order of increasing argument of the central charge, this predicts that the bound state of charge $\gamma_1+\gamma_2$ is stable on the side of the wall where $\arg Z(\gamma_2) < \arg Z(\gamma_1)$, which is equivalent to the Denef stability condition (2.2.1). Moreover, this formula predicts that the bound state will also be a hypermultiplet, since the refined index for a hypermultiplet is $\Omega^{ref}(\gamma;t;y) = \sum_n \Omega_n y^n = 1$ (and all exponents here are 1); this is in agreement with primitive wall crossing (2.2.7).

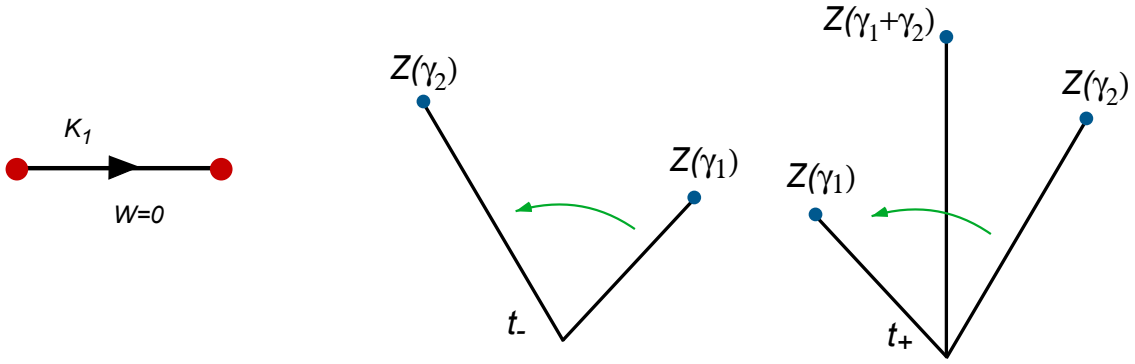

Figure 4.1: Left: the K_1 quiver. Right: the BPS rays of states γ_1, γ_2, and $\gamma_1+\gamma_2$ in the *central charge plane* for stable (t_+) and unstable (t_-) values of moduli.

Note that only states whose central charges actually align at a wall enter the KS wall-crossing formulas.[4] Generically, the charges of these states lie on a 2-dimensional sublattice of Γ. In the present simple example, this sublattice is generated by charges γ_1 and γ_2.

Primitive wall crossing

The pentagon-identity example can easily be generalized to an arbitrary primitive wall crossing. Again, we want to consider two states of charges γ_1 and γ_2 forming a bound state

[4]One could consider other states too, but their corresponding operators would just appear at one side or the other of the product $\prod \mathbf{U}_\gamma$ and their order would not change.

as a wall is crossed, but now $\langle\gamma_1,\gamma_2\rangle$ can be an arbitrary integer. WLOG, we assume

$$\langle\gamma_1,\gamma_2\rangle = I_{12} > 0\,. \tag{4.2.3}$$

Then the motivic wall-crossing formula looks like

$$\mathbf{A}_{\gamma_1}(t_-)\,\mathbf{A}_{\gamma_1+\gamma_2}(t_-)\,\mathbf{A}_{\gamma_2}(t_-) = \mathbf{A}_{\gamma_2}(t_+)\,\mathbf{A}_{\gamma_1+\gamma_2}(t_+)\,\mathbf{A}_{\gamma_1}(t_+)\,. \tag{4.2.4}$$

We expect that $\arg Z(\gamma_1) < \arg Z(\gamma_2)$ on the unstable side of the wall, and so label the LHS of the above formula with the parameter t_-. Let us also assume that the primitive states of charges γ_1 and γ_2 are stable across the wall, so that

$$\mathbf{A}_{\gamma_1}(t_-) = \mathbf{A}_{\gamma_1}(t_+) = \mathbf{A}_{\gamma_1}(t_{ms})\,,$$
$$\mathbf{A}_{\gamma_2}(t_-) = \mathbf{A}_{\gamma_2}(t_+) = \mathbf{A}_{\gamma_2}(t_{ms})\,.$$

The key to understanding this wall-crossing formula (and, indeed, any motivic wall-crossing formula) is to observe that the associative algebra $\mathcal{A}$ generated by $\hat{e}_{\gamma_1}$ and $\hat{e}_{\gamma_2}$ with

$$\hat{e}_{\gamma_1}\hat{e}_{\gamma_2} = q^{I_{12}/2}\hat{e}_{\gamma_1+\gamma_2} = q^{I_{12}}\hat{e}_{\gamma_2}\hat{e}_{\gamma_1} \tag{4.2.5}$$

has filtrations of the form

$$\{1\} \subset \mathcal{A}_{1,0} \subset \mathcal{A}_{1,1} \subset \mathcal{A}_{2,1} \subset \ldots \subset \mathcal{A}_{\infty,\infty} = \mathcal{A}\,, \tag{4.2.6}$$

where at level $\mathcal{A}_{m,n}$ one includes q-polynomials in $\hat{e}_{\gamma_1}$ and $\hat{e}_{\gamma_2}$ of degrees no more than m and n, respectively. For practical purposes, this means that we can consistently expand a formula like (4.2.4) as a series in $\hat{e}_{\gamma_1}$ and $\hat{e}_{\gamma_2}$, keeping any degree we want in these two generators. After commuting all products $\hat{e}_{\gamma_1}^{m'}\hat{e}_{\gamma_2}^{n'}$ in a uniform manner, we can relate the indices $\Omega_n^{mot}(\gamma;t)$ on both sides by simply equating coefficients of like powers.

In this case, let us define

$$\Omega^{mot}(\gamma;t;q) = \sum_{n\in Z}(-q^{1/2})^n\Omega_n^{mot}(\gamma;t)\,, \tag{4.2.7}$$

in analogy to (2.1.31) in the refined case. It is then fairly clear from (4.1.14)-(4.1.17) that for a primitive ray, such that only $k=1$ contributes to (4.1.17), we have

$$\mathbf{A}_\gamma(t) = 1 + \frac{\Omega^{mot}(\gamma;t;q)}{q^{1/2}-q^{-1/2}}\,\hat{e}_\gamma + \ldots. \tag{4.2.8}$$

Substituting this for $\gamma = \gamma_1, \gamma_2, \gamma_1+\gamma_2$ on the two sides of (4.2.4) and keeping only terms of first order in $\hat{e}_{\gamma_1}$ and $\hat{e}_{\gamma_2}$, we find that the coefficients of 1, $\hat{e}_{\gamma_1}$, and $\hat{e}_{\gamma_2}$ agree trivially, whereas the terms of order $\hat{e}_{\gamma_1}\hat{e}_{\gamma_2}$ are

$$\frac{\Omega^{mot}(\gamma_1;t_{ms};q)\Omega^{mot}(\gamma_2;t_{ms};q)}{(q^{1/2}-q^{-1/2})^2}\,\hat{e}_{\gamma_1}\hat{e}_{\gamma_2} + \frac{\Omega^{mot}(\gamma_1+\gamma_2;t_-;q)}{q^{1/2}-q^{-1/2}}\,\hat{e}_{\gamma_1+\gamma_2} = \frac{\Omega^{mot}(\gamma_1;t_{ms};q)\Omega^{mot}(\gamma_2;t_{ms};q)}{(q^{1/2}-q^{-1/2})^2}\,\hat{e}_{\gamma_2}\hat{e}_{\gamma_1} + \frac{\Omega^{mot}(\gamma_1+\gamma_2;t_+;q)}{q^{1/2}-q^{-1/2}}\,\hat{e}_{\gamma_1+\gamma_2} \quad (4.2.9)$$

Using the commutation relations (4.2.5) to (say) push $\hat{e}_{\gamma_2}$ all the way to the left in each term, this immediately implies that

$$\Delta\Omega^{mot}(\gamma_1+\gamma_2;t_-\to t_+;q) = -\frac{q^{I_{12}/2}-q^{-I_{12}/2}}{q^{1/2}-q^{-1/2}}\,\Omega^{mot}(\gamma_1;t_{ms};q)\,\Omega^{mot}(\gamma_2;t_{ms};q)\,, \quad (4.2.10)$$

which is equivalent to the refined primitive formula (2.2.7) upon identifying $\Omega^{mot}(\gamma;t;q) = \Omega^{ref}(\gamma;t;y)$. We can write the prefactor in (4.2.10) as the quantum dimension $[I_{12}]_{q^{1/2}}$.

Semi-primitive wall crossing

To obtain the refined semi-primitive formula (2.2.13), suppose again that states with primitive charges γ_1 and γ_2, satisfying $\langle\gamma_1,\gamma_2\rangle = I_{12} \geq 0$, bind as a wall is crossed at $t = t_{ms}$. This time, however, consider bound states of all charges $\gamma_1 + N\gamma_2$ with $N \geq 1$.[5] Also assume, for simplicity, that no states of charge $\gamma_1 + N\gamma_2$ exist in the spectrum on the unstable side of the wall. Adding in such states is possible, and results in a derivation of the refined version of (2.2.14) rather than (2.2.13), but it demonstrates no new features.

The resulting motivic wall-crossing formula must take the form

$$\mathbf{A}_{\gamma_1}(t_-)\,\mathbf{A}_{\gamma_2}(t_-) = \mathbf{A}_{\gamma_2}(t_+)\times\cdots\mathbf{A}_{\gamma_1+3\gamma_2}(t_+)\,\mathbf{A}_{\gamma_1+2\gamma_2}(t_+)\,\mathbf{A}_{\gamma_1+\gamma_2}(t_+)\,\mathbf{A}_{\gamma_1}(t_+)\,. \quad (4.2.11)$$

As in the primitive case, we assume that

$$\mathbf{A}_{\gamma_1}(t_-) = \mathbf{A}_{\gamma_1}(t_+) = \mathbf{A}_{\gamma_1}(t_{ms})\,,$$
$$\mathbf{A}_{\gamma_2}(t_-) = \mathbf{A}_{\gamma_2}(t_+) = \mathbf{A}_{\gamma_2}(t_{ms})\,,$$

[5]Note that it is not physically possible to have both $\gamma_1 + N\gamma_2$ and $\gamma_1 - N\gamma_2$ bound states. We choose one or the other, and for KS formulas the choices are related by the particle-antiparticle split of the charge lattice.

and will suppress the parameter t in these operators. We want to expand each operator, keeping first-order terms in $\hat{e}_{\gamma_1}$ and all orders in $\hat{e}_{\gamma_2}$. In fact, $\hat{e}_{\gamma_2}$ shall become the generating function variable x. We have:

$$\mathbf{A}_{\gamma_1} = 1 + \frac{\Omega^{mot}(\gamma_1; q)}{q^{1/2} - q^{-1/2}}\, \hat{e}_{\gamma_1} + \dots, \tag{4.2.12}$$

and

$$\begin{aligned}\prod_{N\geq 0}^{\leftarrow} \mathbf{A}_{\gamma_1+N\gamma_2}(t_+) &= 1 + \sum_{N=0}^{\infty} \frac{\Omega^{mot}(\gamma_1 + N\gamma_2; t_+; q)}{q^{1/2} - q^{-1/2}}\, \hat{e}_{\gamma_1+N\gamma_2} + \dots \\ &= 1 + \sum_{N=0}^{\infty} \frac{\Omega^{mot}(\gamma_1 + N\gamma_2; t_+; q)}{q^{1/2} - q^{-1/2}}\, q^{\frac{NI_{12}}{2}} \hat{e}_{\gamma_2}^N \hat{e}_{\gamma_1} + \dots . \end{aligned} \tag{4.2.13}$$

For $\mathbf{A}_{\gamma_2}$, we keep all k terms in (4.1.17) and use the infinite product formula (4.1.22) to write

$$\mathbf{A}_{\gamma_2} = \prod_{k=1}^{\infty} \prod_{n\in\mathbb{Z}} \mathbf{E}\big((-q^{1/2})^n \hat{e}_{\gamma_2}^{\,k}\big)^{\Omega_n^{mot}(k\gamma_2)}. \tag{4.2.14}$$

Now, observe that for any two charges γ, η with $I = \langle \gamma, \eta \rangle > 0$, the quantum dilogarithm satisfies the commutation relation

$$\hat{e}_\gamma\, \mathbf{E}(\hat{e}_\eta) = \hat{e}_\gamma \prod_{r=0}^{\infty} (1 + q^{r+\frac{1}{2}} \hat{e}_\eta)^{-1} = \prod_{r=0}^{\infty} (1 + q^{r+\frac{1}{2}+I} \hat{e}_\eta)^{-1} \hat{e}_\gamma = \left[\prod_{r=0}^{I-1} (1 + q^{r+\frac{1}{2}} \hat{e}_\eta)\right] \mathbf{E}(\hat{e}_\eta)\, \hat{e}_\gamma\,,$$

and similarly for any q-shifted versions of its argument $\hat{e}_\eta$. Therefore, the LHS of (4.2.11) can be written as

$$\begin{aligned} LHS:\ &\left(1 + \frac{\Omega^{mot}(\gamma_1; q)}{q^{\frac{1}{2}} - q^{-\frac{1}{2}}} \hat{e}_{\gamma_1} + \dots\right) \mathbf{A}_{\gamma_2} \\ &= \mathbf{A}_{\gamma_2} \left(1 + \frac{\Omega^{mot}(\gamma_1; q)}{q^{\frac{1}{2}} - q^{-\frac{1}{2}}} \left(\prod_{k=1}^{\infty} \prod_{n\in\mathbb{Z}} \prod_{r=0}^{kI_{12}-1} \big(1 + (-q^{\frac{1}{2}})^n q^{r+\frac{1}{2}} \hat{e}_{\gamma_2}^k\big)^{\Omega_n^{mot}(k\gamma_2)} \right) \hat{e}_{\gamma_1} + \dots \right), \end{aligned}$$

and the RHS as

$$RHS:\ \ \mathbf{A}_{\gamma_2} \left(1 + \frac{1}{q^{\frac{1}{2}} - q^{-\frac{1}{2}}} \sum_{N=0}^{\infty} \Omega^{mot}(\gamma_1 + N\gamma_2; t_+; q) q^{\frac{NI_{12}}{2}} \hat{e}_{\gamma_2}^N \hat{e}_{\gamma_1} + \dots \right).$$

Setting these two sides equal and matching the coefficients of $\hat{e}_{\gamma_1}$ leads to

$$\sum_{N=0}^{\infty} \Omega^{mot}(\gamma_1 + N\gamma_2; t_+; q)\, x^N = \Omega^{mot}(\gamma_1; q) \prod_{k=1}^{\infty} \prod_{n\in\mathbb{Z}} \prod_{r=0}^{kI_{12}-1} \big(1 + (-q^{\frac{1}{2}})^n q^{r+\frac{1}{2}-\frac{I_{12}}{2}} x^k\big)^{\Omega_n^{mot}(k\gamma_2)}, \tag{4.2.15}$$

where

$$x = q^{\frac{I_{12}}{2}} \hat{e}_{\gamma_2}\,. \tag{4.2.16}$$

After a shift in the product in r and the identifications $-q^{1/2} = y$ and $\Omega^{mot} = \Omega^{ref}$, formula (4.2.15) becomes identical to the refined semi-primitive wall-crossing formula (2.2.13).

The careful reader may have wondered why it was consistent to simply declare that there were no $\gamma_1 + N\gamma_2$ states (with $N \geq 2$) when deriving the primitive wall-crossing formula earlier in this section. The answer should now be clear: the primitive formula (4.2.4) can simply be though of as the part of the semi-primitive formula (4.2.11) that is at most first-order in $\hat{e}_{\gamma_2}$. (Or, more properly, this would be true had we added $\gamma_1 + N\gamma_2$ states to the unstable side of the semi-primitive formula.) So there *could* have been higher $\gamma_1 + N\gamma_2$ states in the primitive formula, but we would not have seen them at first order. Likewise, the semi-primitive formula is best thought of as a consistent truncation of the full wall-crossing formula, in a theory with all possible combinations of bound BPS states.

4.3 Examples: $SU(2)$ Seiberg-Witten theory

In this final section, we provide several examples of semi-primitive and non-semi-primitive(!) refined/motivic wall crossing using 4-dimensional $\mathcal{N} = 2$ gauge theory with gauge group $SU(2)$ and $N_f < 4$ flavors of fundamental matter [85, 86]. We first begin with a review of geometric engineering of these theories and their physical moduli spaces and spectra. A much more thorough analysis of physical and motivic wall crossing in $\mathcal{N} = 2$ gauge theory is found in [2].

Gauge theory via string compactification

The construction of 4-dimensional $\mathcal{N} = 2$ gauge theories in the context of string theory compactifications has come to be known as geometric engineering [82]. To obtain $SU(N)$ gauge theory in a type IIA compactification, one begins with a non-compact Calabi-Yau threefold X_N that is a fibration of a 2-complex-dimensional A_{N-1} ADE singularity over $\mathbb{P}^1$. This geometry can arise from a compact $K3$ fibration over $\mathbb{P}^1$ — dual to heterotic string theory on $K3 \times T^2$ [87] — in the limit of $K3$ moduli space where the $K3$ fibers develop an A_{N-1} singularity and all Kähler moduli not associated with the singularity become large. This results in an $SU(N)$ supergravity theory. As the ADE singularity is blown up it

turns into a string of $N-1$ $\mathbb{P}^1$'s fibered over the base $\mathbb{P}^1$, whose sizes correspond to the eigenvalues of the scalar Higgs field of the $SU(N)$ vector multiplet, and break the gauge group generically to $U(1)^{N-1}$. To decouple gravity while keeping the W-boson masses and the four-dimensional gauge coupling constant, one takes the size of the base $\mathbb{P}^1$ to infinity and the overall size of the fiber $\mathbb{P}^1$'s to zero [82]. This finally produces $\mathcal{N}=2$ $SU(N)$ super-Yang-Mills theory on the Coulomb branch.

The resolved local Calabi-Yau X_N has $2N$ compact even-dimensional cycles. Of these, $2N-2$ survive the rigid limit and generate the lattice of electric and magnetic charges in the gauge theory. For example, for $SU(2)$ theory, X_2 can simply be taken as the total space of the canonical line bundle over $\mathbb{P}^1_{(fiber)} \times \mathbb{P}^1_{(base)}$. The dimensions of its compact homology are $(b_0, b_2, b_4, b_6) = (1, 2, 1, 0)$. Electric charges, such as the charge of the W-boson, correspond to $D2$ branes wrapped on the fiber $\mathbb{P}^1$, while magnetic charges of solitons correspond to $D4$ branes wrapped on the entire $\mathbb{P}_1 \times \mathbb{P}_1$, *cf.* [71]. The low-energy theory of the D-branes and the resulting BPS states in the gauge theory can be described by representations of a "subquiver" of the quiver of the Calabi-Yau. In the case of pure $SU(2)$ theory, it is the K_2 Krönecker quiver of Figure 4.2 [71, 88].

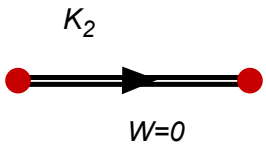

Figure 4.2: The K_2 Krönecker quiver.

To add matter to the $SU(N)$ theories, similar local Calabi-Yau's with extra base $\mathbb{P}^1$'s can be used [89, 90]. The states of the gauge theory are still described by a $2N-2$ sublattice of independent D-brane charges, but the relevant quivers are somewhat more complicated.

Note that there exist type IIB mirrors of these IIA compactifications that encode the Seiberg-Witten curves and the electric-magnetic duality of the gauge theories in a much more explicit manner — though we are less interested in them here because we seek a direct connection with the IIA formalism of Kontsevich-Soibelman. The mirrors of the noncompact Calabi-Yau's X_N's are given by equations of the form

$$xy = H(z, w)\,, \tag{4.3.1}$$

where $H(z,w)=0$ is a Riemann surface whose complex structure corresponds to the Kähler parameters of X_N. In a certain limit of the complex structure (corresponding to decoupling supergravity from the gauge theory) this becomes the Seiberg-Witten curve [82] (see also [63]). BPS states are given by compact $D3$-branes, which descend to non-critical strings on the Riemann surface [91, 92]. It is then easy to identify which branes generate electric and magnetic charges from the corresponding electric and magnetic cycles on the Seiberg-Witten curve.

Moduli spaces and spectra

The moduli space of the Coulomb branch of $SU(2)$ Seiberg-Witten theory is a limit, or slice, of the Kähler moduli space $\mathcal{M}_V$ for the Calabi-Yau X_2 (or the corresponding Calabi-Yau's that include fundamental matter). This moduli space is parametrized by the complex-valued Casimir u of the Higgs field [85, 86]. We draw its structure for theories with $N_f=0,1,2$, and 3 flavors of matter in Figure 4.3, following [93]. When $N_f<4$, the gauge theory is asymptotically free. The large-$|u|$ region corresponds to weak coupling, while the small-u region corresponds to strong coupling, and the two regions are separated by a wall of marginal stability $\mathcal{W}$. The central charge of a state with electric charge q and magnetic charge p is given by

$$Z(p,q;u)=a(u)q+a_D(u)p\,, \tag{4.3.2}$$

where $a(u)$ and $a_D(u)$ can be identified as period integrals on the Seiberg-Witten curve or, more relevantly for us, central charges of $D2$ and $D4$ branes in X_2. The wall of marginal stability is then defined by the condition

$$\arg a(u)=\arg a_D(u)\,,\qquad \text{or}\qquad \frac{a(u)}{a_D(u)}\in\mathbb{R}\,. \tag{4.3.3}$$

Since the charge lattice is two-dimensional, the central charges of *all* states align on $\mathcal{W}$.

In each case $N_f=0,1,2,3$, there are magnetically-charged states that become massless at singular points on $\mathcal{W}$. The BPS spectrum at any point in the weak coupling region can be represented in terms of single-center attractor flows that end on one of these singular points, as well as multi-center attractor flows that split on $\mathcal{W}$ into sums of flows to the singular points [16]. This leads to an infinite spectrum. In contrast, the strong-coupling

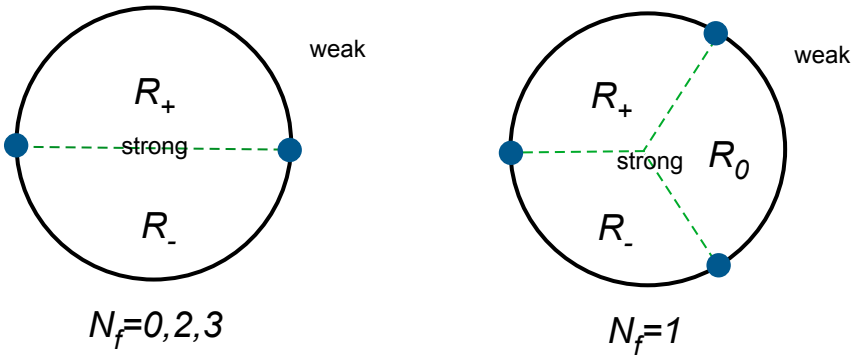

Figure 4.3: The approximate structure of the wall of marginal stability separating weak and strong coupling in the u-plane of Seiberg-Witten theories. We also indicate different local regions within the strong-coupling chamber. For $N_f = 0, 2, 3$, there are BPS states of two different charges that become massless at singularities in the moduli space (the dots here), and for $N_f = 1$ there are three.

spectrum at points inside the wall of marginal stability is simply represented by the finite number of single-center flows to the singularities. Note that the Coulomb branch of an $\mathcal{N} = 2$ gauge theory only possesses a global version of special geometry, as opposed to the local special geometry of supergravity that was described in Section 2.1; nevertheless, a simplified version of the attractor mechanism still functions and BPS states can still be described in terms of attractor flow trees [94].

The spectra of $N_f = 0, 1, 2, 3$ $SU(2)$ theories was carefully derived in [93] using field-theory methods and global properties of the moduli space (see also [91] for an alternative approach). The fundamental electric charge $q = 1$ is *half* the charge of the W-boson. The weak-coupling spectra include the $W^{\pm}$-bosons with $(q, p) = \pm(2, 0)$ and the fundamental quarks with $(q, p) = \pm(1, 0)$. They also contain the monopole and dyons that become massless at singularities on the Coulomb branch and all their conjugates under the monodromy around $u = \infty$ (which must be a symmetry of the weakly-coupled theory). This monodromy acts as

$$M_\infty \,:\, (q, p) \to (q + N_f\, p, p) \tag{4.3.4}$$

on the charge lattice. Altogether, one finds weak-coupling spectra

$$N_f = 0: \quad (2,0)\,,\ (2n,1)\ \ n \in \mathbb{Z}\,, \tag{4.3.5}$$

$$N_f = 1: \quad (2,0)\,,\ (1,0)_2\,,\ (n,1)\ \ n \in \mathbb{Z}\,, \tag{4.3.6}$$

$$N_f = 2: \quad (2,0)\,,\ (1,0)_4\,,\ (n,1)_2\ \ n \in \mathbb{Z}\,, \tag{4.3.7}$$

$$N_f = 3: \quad (2,0)\,,\ (1,0)_6\,,\ (n,1)_4\ \ (2n+1,2)\,,\ n \in \mathbb{Z}\,. \tag{4.3.8}$$

We have suppressed $\pm$ signs for antiparticles, and the subscripts here denote nontrivial multiplicities. At strong-coupling, inside the wall of marginal stability, the spectrum has no single canonical description, due to the nontrivial fibration of the charge lattice over the moduli space. In some of the regions indicated in Figure 4.3, the spectra can be described as

$$N_f = 0: \quad [\mathcal{R}_+]\ \ (2,1)\,,\ (0,1) \qquad [\mathcal{R}_-]\ \ (-2,1)\,,\ (0,1) \tag{4.3.9}$$

$$N_f = 1: \quad [\mathcal{R}_0]\ \ (0,1)\,,\ (-1,1)\,,\ (1,0) \qquad [\mathcal{R}_+]\ \ (2,-1)\,,\ (-1,1)\,,\ (1,0)$$
$$[\mathcal{R}_-]\ \ (0,1)\,,\ (1,1)\,,\ (1,0) \tag{4.3.10}$$

$$N_f = 2: \quad [\mathcal{R}_+]\ \ (1,-1)_2\,,\ (0,1)_2 \qquad [\mathcal{R}_-]\ \ (1,1)_2\,,\ (0,1)_2 \tag{4.3.11}$$

$$N_f = 3: \quad [\mathcal{R}_+]\ \ (-1,2)\,,\ (1,-1)_4 \qquad [\mathcal{R}_-]\ \ (-1,2)\,,\ (0,1)_4\,. \tag{4.3.12}$$

It is also possible to generate the spectra from stable quiver representations. For example, the $N_f = 0$ case is derived from the K_2 quiver of Figure 4.2 in [71] (see also [95]). The $N_f = 1$ case appears in [2].

Refined/motivic wall crossing

We now show that the above physically-determined spectra agree perfectly with motivic wall crossing.

Consider the case $N_f = 0$. Let us choose a basis $\{\gamma_1, \gamma_2\}$ of the charge lattice related to electric and magnetic charges (q, p) by

$$\gamma_1 = (1,-1)\,, \qquad \gamma_2 = (0,1) \tag{4.3.13}$$

with $\langle \gamma_1, \gamma_2 \rangle = 1$ (this is not necessary but will be convenient later). We also choose "particles" (as opposed to antiparticles) to have $q > 0$ for any p, or $q = 0$ and $q > 0$. All

states except the W boson come in hypermultiplets, and should be represented by operators

$$\mathbf{U}_{m,n} := \mathbf{E}_{m\gamma_1+n\gamma_2}(\hat{e}_{\gamma_1+\gamma_2}) \qquad \sim \text{charge } (m, n-m) \tag{4.3.14}$$

in the motivic wall-crossing formula. The W-boson comes in a vector multiplet and should be represented by an operator

$$\mathbf{U}_{2,2}^{\text{vect}} := \mathbf{E}_{2\gamma_1+2\gamma_2}(-q^{1/2}\hat{e}_{2\gamma_1+2\gamma_2})^{-1}\,\mathbf{E}_{2\gamma_1+2\gamma_2}(-q^{-1/2}\hat{e}_{2\gamma_1+2\gamma_2})^{-1}\,. \tag{4.3.15}$$

Near the wall of marginal stability, the central charges of γ_1 and γ_2 coincide. Slightly away from this wall, we either have $\arg Z(2\gamma_1+\gamma_2) < \arg Z(\gamma_2)$ or $\arg Z(2\gamma_1+\gamma_2) > \arg Z(\gamma_2)$. Identifying the former with strong coupling and the latter with weak coupling, the BPS spectra (4.3.5) and (4.3.9) (in region $\mathcal{R}_-$) lead to a predicted motivic wall-crossing formula

$$\mathbf{U}_{2,1}\,\mathbf{U}_{0,1} \stackrel{?}{=} \mathbf{U}_{0,1}\,\mathbf{U}_{2,3}\,\mathbf{U}_{4,5}\,\mathbf{U}_{6,7}\cdots\mathbf{U}_{2,2}^{\text{vect}}\cdots\mathbf{U}_{6,5}\,\mathbf{U}_{4,3}\,\mathbf{U}_{2,1}\,. \tag{4.3.16}$$

This formula is in fact true. It can be checked algebraically, order by order in $\hat{e}_{\gamma_1}$ and $\hat{e}_{\gamma_2}$. (This is in fact one reason for our choice of basis (4.3.13) — so no negative powers of $\hat{e}$'s appear, making it possible to easily truncate series at any degree.) It is also possible to prove (4.3.16) directly by deriving motivic invariants from the K_2 quiver [2]. After the arguments in Section 4.2, it may not be too surprising that this formula works; however, in our research it preceded the proof of refined wall crossing from motivic wall crossing, and provided the first hint that the factorization property (4.1.16) should hold.

Using the same basis (4.3.13) and choice of particles vs. antiparticles, the BPS spectra for $N_f = 1$ and $N_f = 2$ theories predict motivic wall-crossing formulas

$$N_f = 1: \quad \mathbf{U}_{1,0}\,\mathbf{U}_{1,1}\,\mathbf{U}_{0,1} = \mathbf{U}_{0,1}\,\mathbf{U}_{1,2}\,\mathbf{U}_{2,3}\,\mathbf{U}_{3,4}\cdots\mathbf{U}_{1,1}^{2}\,\mathbf{U}_{2,2}^{\text{vect}}\cdots\mathbf{U}_{3,2}\,\mathbf{U}_{2,1}\,\mathbf{U}_{1,0} \tag{4.3.17}$$

$$N_f = 2: \quad \mathbf{U}_{1,0}^{2}\,\mathbf{U}_{0,1}^{2} = \mathbf{U}_{0,1}^{2}\,\mathbf{U}_{1,2}^{2}\,\mathbf{U}_{2,3}^{2}\,\mathbf{U}_{3,4}^{2}\cdots\mathbf{U}_{1,1}^{4}\,\mathbf{U}_{2,2}^{\text{vect}}\cdots\mathbf{U}_{3,2}^{2}\,\mathbf{U}_{2,1}^{2}\,\mathbf{U}_{1,0}^{2}\,. \tag{4.3.18}$$

With a slightly different choice of particles vs. antiparticles, the following is obtained,

$$N_f = 3: \quad \mathbf{U}_{1,-1}\,\mathbf{U}_{0,1}^{4} = \mathbf{U}_{0,1}^{4}\,\mathbf{U}_{1,3}\,\mathbf{U}_{1,2}^{4}\,\mathbf{U}_{3,5}\,\mathbf{U}_{2,3}^{4}\cdots\mathbf{U}_{1,1}^{6}\,\mathbf{U}_{2,2}^{\text{vect}}\cdots\mathbf{U}_{2,1}^{4}\,\mathbf{U}_{3,1}\,\mathbf{U}_{1,0}^{4}\,\mathbf{U}_{1,-1}\,. \tag{4.3.19}$$

Algebraically, the validity of all these formulas follows directly from the validity of (4.3.16). They can be derived by commuting operators $\mathbf{U}_{1,1}$ through the infinite products on the RHS using the pentagon relation; a sample proof for $N_f = 1$ appears at the end of this section.

Formulas (4.3.17), (4.3.18), and (4.3.19) correspond to the strong-coupling spectra in regions $\mathcal{R}_0$, $\mathcal{R}_+$, and $\mathcal{R}_-$, respectively. This choice of regions is correlated to the choice of split between particles and antiparticles. For example, for $N_f = 1$ the following formulas also hold:

$$N_f = 1\,[\mathcal{R}_+]: \quad \mathbf{U}_{2,1}\,\mathbf{U}_{1,1}\,\mathbf{U}_{-1,0} = \mathbf{U}_{-1,0}\,\mathbf{U}_{0,1}\,\mathbf{U}_{1,2}\,\mathbf{U}_{2,3}\,\mathbf{U}_{3,4}\cdots\mathbf{U}_{1,1}^2\,\mathbf{U}_{2,2}^{\text{vect}}\cdots\mathbf{U}_{3,2}\,\mathbf{U}_{2,1}$$
$$N_f = 1\,[\mathcal{R}_-]: \quad \mathbf{U}_{0,-1}\,\mathbf{U}_{1,1}\,\mathbf{U}_{1,2} = \mathbf{U}_{1,2}\,\mathbf{U}_{2,3}\,\mathbf{U}_{3,4}\cdots\mathbf{U}_{1,1}^2\,\mathbf{U}_{2,2}^{\text{vect}}\cdots\mathbf{U}_{3,2}\,\mathbf{U}_{2,1}\,\mathbf{U}_{1,0}\,\mathbf{U}_{0,-1}\,.$$

Altogether, we find that the physical derivations of refined BPS spectra agree perfectly with mathematical motivic formulas.

Proving $N_f = 0 : N_f = 1, 2, 3$

The key to deriving (4.3.17), (4.3.18), (4.3.19) from (4.3.16) is to observe that all terms on the RHS are of the form $\mathbf{U}_{k,k+1}$ or $\mathbf{U}_{k+1,k}$, and that, due to the pentagon identity (4.1.21),

$$\mathbf{U}_{1,1}\,\mathbf{U}_{k,k+1} = \mathbf{U}_{k,k+1}\,\mathbf{U}_{k+1,k+2}\,\mathbf{U}_{1,1}\,, \qquad \mathbf{U}_{k+1,k}\,\mathbf{U}_{1,1} = \mathbf{U}_{1,1}\,\mathbf{U}_{k+2,k+1}\,\mathbf{U}_{k+1,k}\,. \quad (4.3.20)$$

Therefore, fundamental quark operators $\mathbf{U}_{1,1}$ can be commuted through the semi-infinite products on the RHS of (4.3.16) in pairs to obtain the other formulas. For example, for $N_f = 1$ we have

$$\begin{aligned}
&\mathbf{U}_{0,1}\,\mathbf{U}_{1,2}\,\mathbf{U}_{2,3}\,\mathbf{U}_{3,4}\,\mathbf{U}_{4,5}\cdots\mathbf{U}_{1,1}^2\,\mathbf{U}_{2,2}^{\text{vect}}\cdots\mathbf{U}_{5,4}\,\mathbf{U}_{4,3}\,\mathbf{U}_{3,2}\,\mathbf{U}_{2,1}\,\mathbf{U}_{1,0} \\
&\qquad = \mathbf{U}_{1,1}\left[\,\mathbf{U}_{0,1}\,\mathbf{U}_{2,3}\,\mathbf{U}_{4,5}\cdots\mathbf{U}_{2,2}^{\text{vect}}\cdots\mathbf{U}_{6,5}\,\mathbf{U}_{4,3}\,\mathbf{U}_{2,1}\,\right]\mathbf{U}_{1,1}\,\mathbf{U}_{1,0} \\
&\qquad \overset{N_f=0}{=} \mathbf{U}_{1,1}\left[\,\mathbf{U}_{2,1}\,\mathbf{U}_{0,1}\,\right]\mathbf{U}_{1,1}\,\mathbf{U}_{1,0} \\
&\qquad = \mathbf{U}_{1,1}\,\mathbf{U}_{2,1}\,\mathbf{U}_{1,0}\,\mathbf{U}_{0,1} \\
&\qquad = \mathbf{U}_{1,0}\,\mathbf{U}_{1,1}\,\mathbf{U}_{0,1}\,.
\end{aligned}$$

The last two lines follow by further applications of the pentagon identity (4.1.21).